ACS APPLIED NANO MATERIALS

www.acsanm.org

Review

Nanoparticle-Based Strategies to Combat COVID-19

Riddhiman Medhi, Pannaree Srinoi, Nhat Ngo, Hung-Vu Tran, and T. Randall Lee*

Cite This: *ACS Appl. Nano Mater.* 2020, 3, 8557−8580

Read Online

ACCESS | Metrics & More | Article Recommendations

ABSTRACT: Coronavirus disease 2019 (COVID-19) is the worst pandemic disease of the current millennium. This disease is caused by the highly contagious severe acute respiratory syndrome coronavirus 2 (SARS-CoV-2), which first exhibited human-to-human transmission in December 2019 and has infected millions of people within months across 213 different countries. Its ability to be transmitted by asymptomatic carriers has put a massive strain on the currently available testing resources. Currently, there are no clinically proven therapeutic methods that clearly inhibit the effects of this virus, and COVID-19 vaccines are still in the development phase. Strategies need to be explored to expand testing capacities, to develop effective therapeutics, and to develop safe vaccines that provide lasting immunity. Nanoparticles (NPs) have been widely used in many medical applications, such as biosensing, drug delivery, imaging, and antimicrobial treatment. SARS-CoV-2 is an enveloped virus with particle-like characteristics and a diameter of 60−140 nm. Synthetic NPs can closely mimic the virus and interact strongly with its proteins due to their morphological similarities. Hence, NP-based strategies for tackling this virus have immense potential. NPs have been previously found to be effective tools against many viruses, especially against those from the *Coronaviridae* family. This Review outlines the role of NPs in diagnostics, therapeutics, and vaccination for the other two epidemic coronaviruses, the 2003 severe acute respiratory syndrome (SARS) virus and the 2012 Middle East respiratory syndrome (MERS) virus. We also highlight nanomaterial-based approaches to address other coronaviruses, such as human coronaviruses (HCoVs); feline coronavirus (FCoV); avian coronavirus infectious bronchitis virus (IBV); coronavirus models, such as porcine epidemic diarrhea virus (PEDV), porcine reproductive and respiratory syndrome virus (PRRSV), and transmissible gastroenteritis virus (TGEV); and other viruses that share similarities with SARS-CoV-2. This Review combines the salient principles from previous antiviral studies with recent research conducted on SARS-CoV-2 to outline NP-based strategies that can be used to combat COVID-19 and similar pandemics in the future.

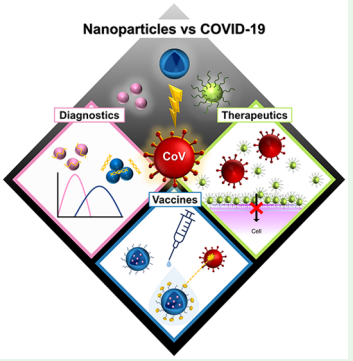

KEYWORDS: *COVID-19, SARS-CoV-2, coronavirus, nanoparticles, diagnostics, drugs, vaccines, antiviral therapy*

1. INTRODUCTION

A novel coronavirus named severe acute respiratory syndrome coronavirus 2 (SARS-CoV-2) caused an outbreak of the pulmonary disease called coronavirus disease 2019 (COVID-19), starting in December 2019 in the city of Wuhan in China.[1−3] The primary symptoms of COVID-19 include fever, severe respiratory illness, pneumonia, and dyspnea.[1,2] Since the initial outbreak, efficient human-to-human transmission has led to exponential growth of the virus, infecting millions of people.[1,4] The World Health Organization (WHO) declared a Public Health Emergency of International Concern (PHEIC) on 30 January 2020 and declared the outbreak a pandemic on 11 March 2020.[3,4] At the time of publication, SARS-CoV-2 has infected tens of millions of people across the globe, leading to more than 800,000 deaths worldwide.

The fight against a viral pandemic needs multipronged scientific approaches. The first requirement is the diagnostic detection of the virus. The development of fast and effective testing methods enables contact tracing and isolation of infected people, slowing the spread of the virus. Particularly with SARS-CoV-2, which spreads quickly through asymptomatic carriers,[5] large-scale testing is required to obtain a complete picture of viral spread. The testing methods must be accurate, suitable for mass production, inexpensive, and easy to deploy and use. Second, there is a need for therapeutic interventions that can effectively cure or reduce the effects of the virus. Therapeutics in the form of drugs and treatment strategies are essential to reduce the morbidity and mortality caused by the virus. Third, vaccines must be developed to help create antibodies, leading to eventual herd immunity. Vaccination has been able to eradicate various epidemic diseases, including smallpox, polio, and tuberculosis, in many countries.[6] However, the development of vaccines against most viral diseases has proven to be challenging. Researchers are yet to develop a vaccine for human immunodeficiency virus

Received: July 21, 2020
Accepted: August 26, 2020
Published: August 26, 2020

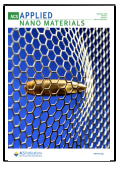

https://dx.doi.org/10.1021/acsanm.0c01978
ACS Appl. Nano Mater. 2020, 3, 8557−8580

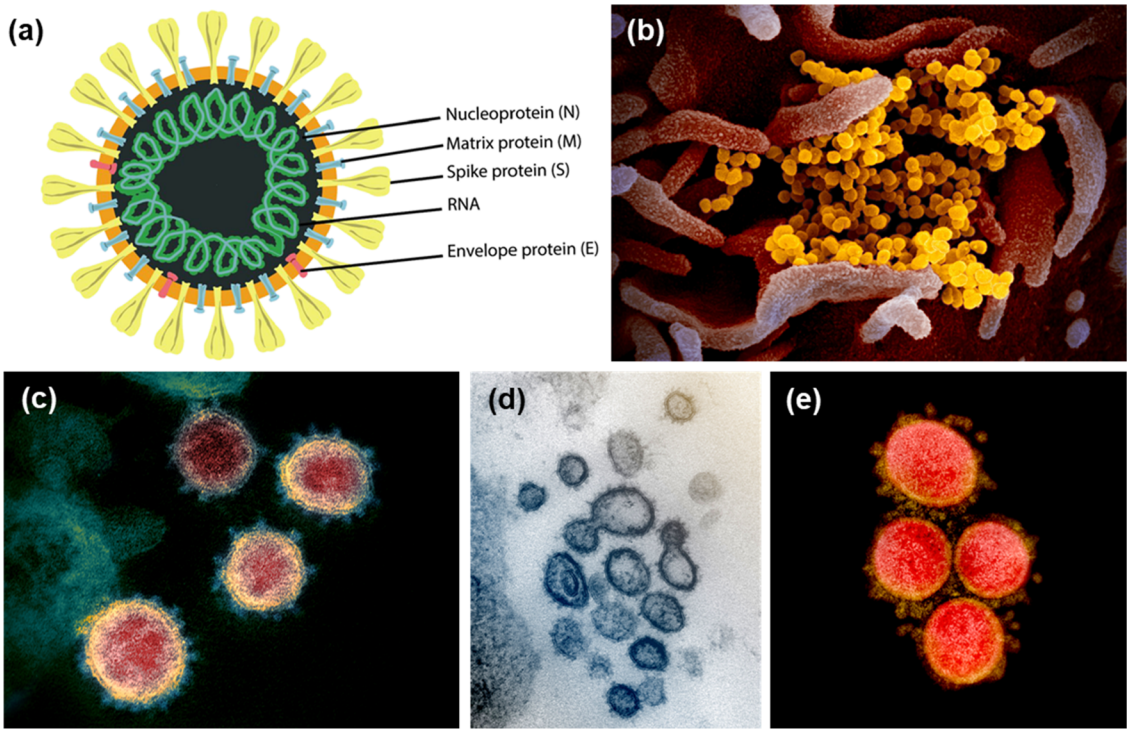

Figure 1. (a) The SARS-CoV-2 structure is illustrated, with its structural viral proteins indicated. Reproduced with permission from ref 12. Copyright 2020 American Chemical Society. (b) Scanning electron microscopy (SEM) image showing the particulate nature of SARS-CoV-2 (yellow) isolated from a patient in the U.S., emerging from the surface of cells (pink) cultured in the laboratory. Image captured and colorized at NIAID's Rocky Mountain Laboratories (RML) in Hamilton, Montana. Credit: NIAID-RML. (c–e) Transmission electron microscopy (TEM) images show SARS-CoV-2 isolated from a patient in the U.S. Virus particles are shown emerging from the surface of cells cultured in the laboratory. The crown-like spikes on the outer edge of the virus particles give coronaviruses their name. Image captured and colorized at NIAID's RML in Hamilton, Montana. Credit: NIAID-RML.

(HIV), which has caused over 40 million deaths to date.[7] Similarly, respiratory viral diseases (e.g., influenza) infect 3–5 million people and cause 290 000–650 000 deaths annually.[8] The 2003 SARS outbreak, which infected ~8300 people with a mortality rate of ~10%, eventually subsided in the summer, but there were no vaccines found at that time.[9] In 2012, the Middle East respiratory syndrome (MERS) virus affected at least 27 countries with a very high mortality rate of 35%.[10,11] Since then, much progress has been made in the field of vaccination against coronaviruses, the principles of which apply to SARS-CoV-2 as well. SARS-CoV-2 exhibits ~80 and 50% similarity with the genomes of SARS-CoV and MERS-CoV, respectively.[12] All coronaviruses are zoonotic viruses, and similar to the 2003 SARS-CoV, SARS-CoV-2 also has a zoonotic origin, having emerged from bats.[9] SARS-Cov-2 has approximately 96% similarity to the bat coronavirus BatCoV RaTG13.[13]

SARS-CoV-2, a positive-sense single-stranded ribonucleic acid ((+)ssRNA) virus from the *Coronaviridae* family, is covered by an envelope with protein spikes.[12] As illustrated in Figure 1a, the four structural proteins of SARS-CoV-2 are spike surface glycoprotein (*S*), small envelope protein (*E*), matrix protein (*M*), and nucleocapsid protein (*N*). Official electron microscopy images released by the U.S. National Institute of Allergy and Infectious Diseases (NIAID), shown in Figures 1b–e, show the morphology and structure of SARS-CoV-2. SARS-CoV-2 particles have a diameter ranging from 60 to 140 nm.[12,14] Due to the particulate nature, morphology, and size domain of SARS-CoV-2, nanoparticle (NP)-based strategies present a powerful approach for tackling this virus. Recently, NPs have been widely used in many medical applications, such as biosensing, drug delivery, imaging, and antimicrobial treatment.[15–18] Various NPs have been shown to be effective tools for the detection and inhibition of and vaccination against coronaviruses.[19,20] This Review describes how we can build on the NP-based strategies used against viruses from the *Coronaviridae* family to develop tests, therapeutics, and vaccines to fight SARS-CoV-2.

2. NANOPARTICLES FOR DIAGNOSTICS

Most viral RNA detection methods are based on the reverse transcription polymerase chain reaction (RT-PCR) due to its simplicity, high sensitivity, and high specificity based on the exponential increase in RNA produced during the operation.[21,22] Although RT-PCR methods are widely known as the standard methods for coronavirus detection, there are some limitations that need to be addressed, including low extraction efficiency, the use of time-consuming processes, and false positives caused by contamination.[23] Regarding the improvement of virus detection efficiency, due to their high surface area and ultrasmall size, NPs have been applied not only in RT-PCR methods but also other virus detection methods, such as an enzyme-linked immunosorbent assay (ELISA) and reverse transcription loop-mediated isothermal amplification (RT-LAMP).[24,25] Various kinds of NPs have been studied in the context of virus detection, including metal NPs, carbon nanotubes, silica NPs, quantum dots (QDs), and polymeric NPs.[20,26] Among them, metal NPs, metal nanoislands (NIs), magnetic NPs (MNPs), and QDs have been applied to coronavirus detection. Most of these diagnostic methods are

https://dx.doi.org/10.1021/acsanm.0c01978
ACS Appl. Nano Mater. 2020, 3, 8557–8580

Table 1. Nanoparticles for Coronavirus Diagnostics

NPs	conjugate	size (nm)	principles	detection techniques	virus	target molecules	detection limit [time]	key takeaways for COVID-19	ref.
AuNPs	citrate ion	13	LSPR	colorimetric sensor	**SARS**	viral RNA	4.3 nM [2 min]	aggregation of AuNPs by formation of dsDNA	27
	citrate ion	19	LSPR	colorimetric sensor	**MERS**	viral RNA	1 pmol/μL [10 min]	preventing aggregation of AuNPs by thiol−dsDNA	28
	streptavidin	-	LSPR and RT-LAMP	colorimetric sensor on strip	**MERS**	viral RNA	1×10^1 copies/μL [35 min]	doubly labeled viral RNA amplicons binding to both AuNPs and antibody-coated detection strip	29
	ASOs	-	LSPR	colorimetric sensor	**SARS-CoV-2**	N gene	0.18 ng/μL [10 min]	aggregation of AuNPs induced by viral N-gene	30
	-	50	electronic	electrochemical immonosensor	**HCoV, MERS**	virus	0.4 pg/mL, 1.0 pg/mL [20 min]	viral antigen immobilized to AuNP surface on electrodes	31
AuNIs	-	40	PPT and PCR	gel electrophoresis	**MERS**	viral cDNA	0.1 ng/μL [-]	ultrafast PCR for rapid cDNA amplification	32
	-	-	LSPR and PPT	LSPR sensor	**SARS-CoV-2**	viral RNA	0.22 pM [-]	high selectivity to target virus, using cDNA receptors	32
AgNPs	citrate ion	19	LSPR	colorimetric sensor	**MERS, MTB, HPV**	viral cDNA	1.53 nM, 1.27 nM, 1.03 nM [-]	cDNAs preventing aggregation of AgNPs induced by acpcPNA	33
SMNPs	silica and oligonucleotide sequences	-	magnetic and PCR	fluorescent sensor	**SARS**	viral cDNA	2.0×10^3 copies [6 h]	capturing and enriching viral target cDNA based on probe-functionalized MNPs	34
MNPs	PC	10	magnetic and RT-PCR	-	**SARS-CoV-2**	viral RNA	10 copies [30 min]	capturing and enriching viral target RNA based on probe-functionalized MNPs	35
QDs-605	RNA aptamer	-	optical	fluorescent sensor	**SARS**	*N* protein	0.1 pg/mL [1 h]	high sensitivity of immobilized target viral *N* protein	36
CdTe QDs and AuNPs	viral antibodies	6−7 (QDs), 50 (AuNPs)	optical and LSPR	chiro-optical sensor	**H5N1, H4N6, FAdVs-9**	viral recombinant protein	1 pg/mL [-]	plasmon−exciton interaction of QDs and star-shaped AuNPs	37
ZrQDs and MPNPs	viral antibodies	2−3 (QDs), 50 (MPNPs)	optical, LSPR, and magnetic	optical sensor	**IBV**	virus	79 EID/50 μL [-]	combination of plasmon−exciton interaction with magnetic separation	38

[a]Abbreviations: LSPR: localized surface plasmon resonance, dsdna: double-stranded DNA, ASOs: antisense oligonucleotides, cDNA: complementary DNA, acpcPNA: pyrrolidinyl peptide nucleic acid, SMNPs: silica-coated superparamagnetic nanoparticles, PPT: plasmonic photothermal, PC: poly(amino ester) with carboxyl groups, MPNPs: magnetoplasmonic nanoparticles.

https://dx.doi.org/10.1021/acsanm.0c01978
ACS Appl. Nano Mater. 2020, 3, 8557−8580

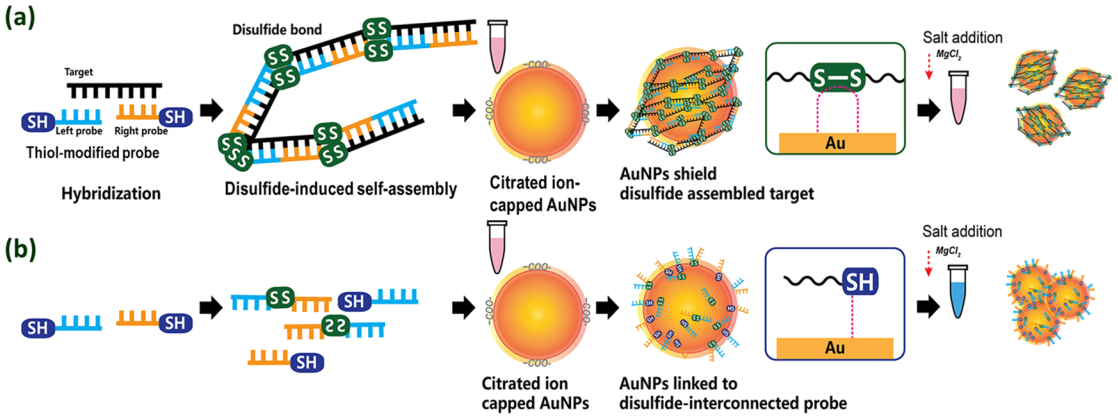

Figure 2. Colorimetric detection of RNAs based on a disulfide-induced self-assembly process. (a) Procedures for preventing salt-induced aggregation of AuNPs by disulfide-induced self-assembly of long thiol-modified dsDNAs in the presence of targets. (b) Salt-induced aggregation of AuNPs in the absence of targets. Adapted with permission from reference 28. Copyright 2019 American Chemical Society.

based on colorimetric, electrochemical, fluorescence, and optical detection techniques. Table 1 provides a summary of the NPs used in the diagnostic detection of coronaviruses.

2.1. Metal Nanoparticles and Metal Nanoislands. Most metal NP-based virus detection techniques were designed based on the unique optical and electrical properties of metal NPs. In particular, noble metal NPs, such as gold, silver, and copper, have unique optical properties called localized surface plasmon resonance (LSPR). LSPR has been utilized in biosensing applications due to the tunable light absorption and scattering wavelength in the visible region. The change in the LSPR extinction maxima of metal NPs depends on the refractive index of the surrounding media and the degree of NP aggregation, which are important factors for the use of these NPs in biological applications.[39−41] Gold NPs (AuNPs) are the most common NPs used in diagnostic detection of viruses due to their unique optical properties, stability, and biocompatible properties.[42−44] Due to the LSPR effect, the aggregation of AuNPs causes a redshift in the LSPR peak position, resulting in an obvious change in the solution color from red to blue, which can be observed with the naked eye. This phenomenon is caused by the plasmonic coupling among the neighboring NPs when the colloidal NPs aggregate.[45]

The applications of AuNPs in virus detection have been reported.[42] AuNPs are also the most common metal NPs that have been used for coronavirus diagnostics. The use of AuNPs in colorimetric detection of SARS-CoV has been reported.[27] In this study, the difference in the electrostatic properties of single- and double-stranded DNA (ssDNA and dsDNA) was the foundation of the method. Specifically, ssDNA or ssRNA could interact with citrate ions on the surface of AuNPs and stabilize the particles even when salt was added into the solution, while the presence of dsDNA caused aggregation of AuNPs under the same conditions. Based on this finding, Li and Rothber designed a simple colorimetric hybridization assay to detect SARS-CoV based on the formation of dsDNA from viral ssRNA.[27] This colorimetric detection method confirmed the formation of dsDNA with a target concentration of 4.3 nM. Essentially, the results were observed within 10 min without the need for any complicated instrument. In a different approach, the formation of long dsDNA molecules from reactions of the target viral RNAs with a pair of thiol-functionalized probes showed the ability to stabilize AuNPs under positive electrolyte conditions.[28] In the presence of the target viral RNAs of MERS-CoV, the formation of disulfide bonds between the thiol-functionalized probes, which were designed to interact with target viral RNA, caused a self-assembly process to produce long thiol-modified dsDNA molecules on the gold surface. These monolayers of the long polymer-type structures of thiol-modified dsDNA on the surface prevented the AuNPs from aggregating under positive electrolyte conditions when $MgCl_2$ was added into the solution (Figure 2a). On the other hand, the thiol-modified probes, without interaction with the target molecules, stayed on the AuNP surface in individual (monomeric) or dimeric molecules, formed via a disulfide formation reaction. Due to their short chain length, both monomers and dimers of the thiol-modified probes could not prevent the aggregation of AuNPs when salt was added, as shown in Figure 2b. This colorimetric reaction led to a change in the AuNP colloidal solution color in the presence of MERS-CoV at as low as 1 pmol/μL, and the detection process took only 10 min without additional procedures.

AuNPs can be further functionalized with biomolecules to modify their surface properties. For example, colloidal AuNPs conjugated with streptavidin were used for an RT-LAMP combined with a vertical flow visualization strip (RT-LAMP-VF) assay for MERS-CoV nucleic acid detection.[29] In this study, viral RNA was amplified by RT-LAMP, followed by a labeling process to form biotin/fluorescein isothiocyanate (FITC)-labeled amplicons. These amplicons can bind to streptavidin-functionalized AuNPs to generate a complex via biotin−streptavidin interactions. This complex showed color formation when captured by an anti-FITC antibody coated on the detection strip. The formation of the complex on the strip was visible to the naked eye within 35 min. The detection limit of this technique is equivalent to 10 copies/μL of MERS-CoV RNA. Moreover, the method showed high specificity for MERS-CoV without cross-reactivity with various other CoVs, such as HCoV-HKU1, HCoV-HKU4, SARS-CoV, HCoV-229E, and HCoV-OC43. Recently, designed thiol-modified antisense oligonucleotides (ASOs) were functionalized on AuNPs for colorimetric detection of the N gene (nucleocapsid phosphoprotein) of SARS-CoV-2.[30] Specifically, in the presence of the N gene of SARS-CoV-2, the thiol-modified ASO-capped AuNPs agglomerated, which caused a change in the color of the ASO-capped AuNP colloidal solution.

https://dx.doi.org/10.1021/acsanm.0c01978
ACS Appl. Nano Mater. 2020, 3, 8557−8580

Moreover, ribonuclease H (RNaseH) was added to the solution to cause visually detectable precipitation of agglomerated ASO-capped AuNPs. This method yielded the result within 10 min after the RNA isolation process. Additionally, the detection limit of this method was 0.18 ng/μL.

In addition to plasmon-based virus detection, AuNPs have been applied to electrochemical detection of coronaviruses. Layqah and Eissa reported the use of AuNPs to modify carbon array electrodes in electrochemical biosensors for both MERS-CoV and HCoV detection.[31] In this method, a viral antigen (recombinant spike protein S1 of MERS-CoV or Oc43 N of HCoV) is immobilized to the surface of AuNPs on the working electrodes. When a fixed amount of the corresponding viral antibody is added to the sample, the antibody binds to the immobilized antigen, decreasing the square wave voltammetry (SWV) reduction peak current. In the presence of virus, the change in current is different due to competition between the virus and immobilized antigen for binding to the antibody. Hence, the virus is detected based on the measured change in current in competitive immunoassays. The deposition of gold improves the electron transfer rate and increases the surface area of the electrode, resulting in high sensitivity of virus detection.[31] Specifically, this detection method was able to detect both MERS-CoV and HCoV with detection limits of 1.0 and 0.4 pg/mL, respectively. The detection process yielded results within 20 min. The method can be used for artificial nasal samples as well as to detect MERS-CoV and HCoV simultaneously.

Recently, Lee et al. developed a method for the detection of MERS-CoV based on nanoplasmonic on-chip PCR.[32] In this study, nanoplasmonic pillar arrays (NPAs) constructed from gold NIs (AuNIs) deposited on the top and side walls of glass nanopillar arrays were used to enhance the light absorption efficiency of the detection chip. Hence, ultrafast PCR thermal cycling was achieved via enhanced plasmonic photothermal heating generated via excitation of surface electrons of AuNIs by a white light-emitting diode (LED). When the LED was off, efficient heat diffusion through the NPAs allowed expeditious cooling of the PCR mixture. Consequently, this method required only 3 min and 30 s for rapid amplification of complementary DNA (cDNA) of MERS-CoV at a concentration of 0.1 ng/μL. However, the method could yield results very rapidly due to the use of gel electrophoresis for visualization of the amplicons of target viral cDNAs after the PCR. Interestingly, a faster detection technique was utilized by Wang and co-workers in a recently reported dual-function plasmonic photothermal biosensor for SARS-CoV-2 detection.[46] This biosensor combined the plasmonic photothermal (PPT) effect and LSPR biosensing technique for highly accurate detection of SARS-CoV-2 by targeting the viral RNA-dependent RNA polymerase (RdRp) sequence. Two-dimensional AuNIs (5.0−5.2 nm thick) were functionalized with thiol-modified cDNA receptors of viral gene sequences (RdRp-COVID or RdRp-SARS) to create microfluidic LSPR sensor chips (Figure 3a). Localized thermoplasmonic heating significantly improved the hybridization speed of viral gene sequence targets with their cDNA receptors immobilized on the sensor chips, enhancing the sensing performance. Importantly, this sensor can distinguish SARS-CoV and SARS-CoV-2 due to the partial mismatch between the sequences of the SARS-CoV and SARS-CoV-2 cDNA receptors, as shown in Figure 3b,c.[46] This method exhibited high sensitivity toward SARS-CoV-2 sequences at a concentration of 0.22 pM.

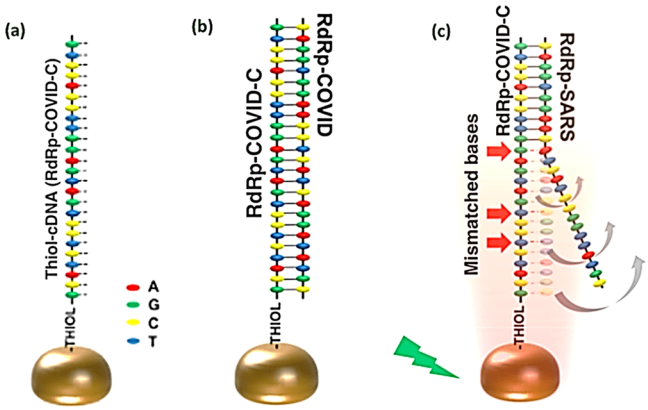

Figure 3. Schematic illustrations of (a) cDNA-receptor-functionalized AuNI based on the reaction with thiol−cDNA ligands, (b) the hybridization of two complementary strands, and (c) the hybridization of two partially matched sequences. Adapted with permission from reference 46. Copyright 2020 American Chemical Society.

Although AuNPs are the most common metal NPs used in virus detection, several studies have suggested the use of other metal NPs. Silver NPs (AgNPs) have been used in paper-based analytical devices (PADs) for MERS-CoV detection.[33] The device can also be applied in the diagnosis of other bacteria and viruses, such as *Mycobacterium tuberculosis* (MTB) and human papillomavirus (HPV). In this study, the authors used pyrrolidinyl peptide nucleic acid (acpcPNA)-induced aggregation of AgNPs to design a colorimetric assay. Specifically, the cationic acpcPNA probes can bind to negative citrate ions on the surface of AgNPs, inducing NP aggregation together with a change in color. On the other hand, in the presence of viral target cDNAs, acpcPNAs preferred to interact with the target cDNAs to form dsDNAs and stayed separate from AgNPs in the solution, leading to no significant color change.[33] The paper-based device exhibited high sensitivity, with detection limits of 1.53, 1.27, and 1.03 nM for MERS-CoV, MTB, and HPV, respectively.

2.2. Magnetic Nanoparticles. Magnetic NPs (MNPs) play an important role in the separation of viral RNA from solution before the diagnosis process.[47,48] The most common MNPs that have drawn attention in the biological application field are iron oxide NPs due to their high magnetic efficiency and simple synthesis approaches.[49,50] Regarding coronavirus detection, Gong et al. used silica-coated superparamagnetic NPs (SMNPs) in PCR-based assays to improve the selectivity of the target cDNA of SARS-CoV in the separation process.[34] Specifically, silica-coated SMNPs were conjugated with oligonucleotide probes for capturing viral target cDNAs to produce magnetic-conjugated dsDNA complexes. The magnetic-conjugated dsDNA was separated from other components by using simple magnetic separation before dehybridization to form enriched cDNAs.[34] The viral enriched cDNA was amplified through PCR followed by isolation via another magnetic separation step. The amplified viral target cDNA was detected by a sandwich hybridization assay with silica-coated fluorescent NP (SFNP)-based signaling probes. The technique can detect the target cDNA with a detection limit of 2.0×10^3 copies within 6 h.

Recently, MNPs have been applied to SARS-CoV-2 detection. Several studies have reported the use of iron oxide

https://dx.doi.org/10.1021/acsanm.0c01978
ACS Appl. Nano Mater. 2020, 3, 8557−8580

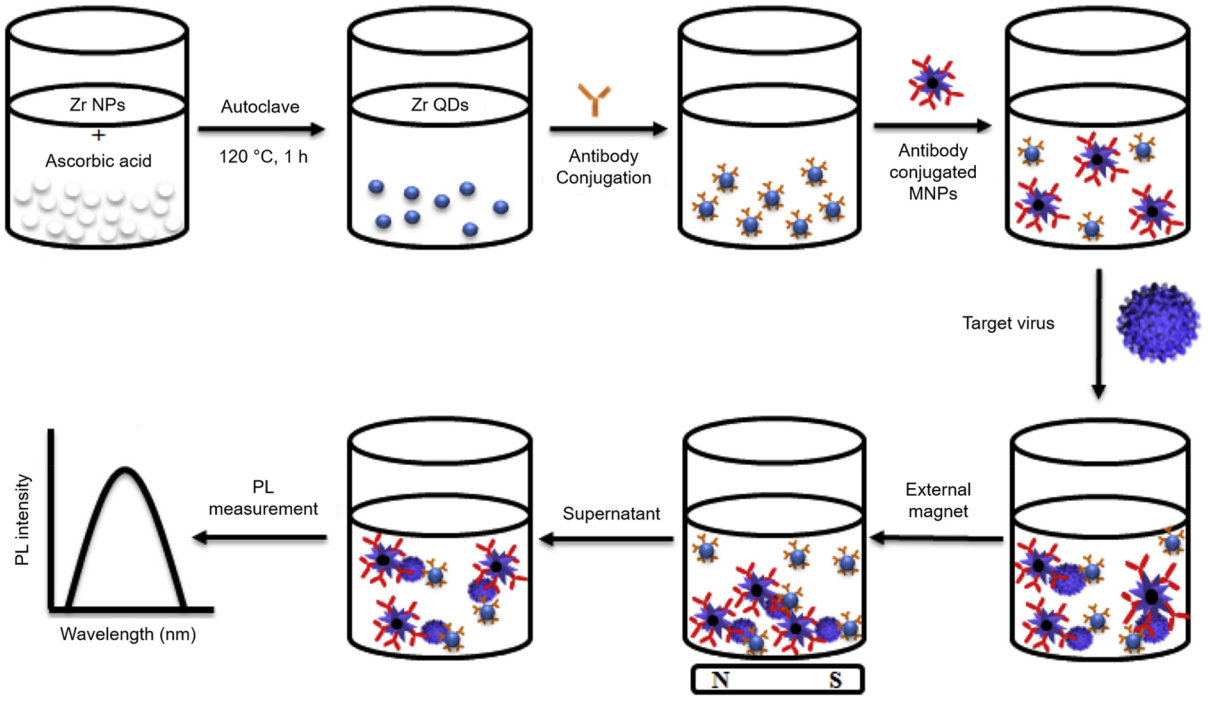

Figure 4. Schematic illustration of the formation of ZrQDs and Fe_3O_4@Au MPNP nanohybrid structures for magnetoplasmonic−fluorescent virus detection. Adapted with permission from reference 38. Copyright 2018 Elsevier.

coated with silica for RNA extraction from patient samples.[51,52] Furthermore, other functional groups have been reported to have strong affinity for viral RNAs. Zhou, Yu, and co-workers reported a viral RNA extraction method using poly(amino ester) with carboxyl group (PC)-coated MNPs (pcMNPs).[35] SARS-CoV-2 RNA was captured and enriched by pcMNPs to produce pcMNP−RNA complexes. Due to the magnetic property of pcMNPs, the pcMNP−RNA complexes were easily extracted from the solution by applying an external magnetic force. Interestingly, the pcMNP−RNA complexes can be immediately used in the following RT-PCR process for viral RNA amplification without the use of an elution step. The pcMNP-based extraction method exhibited high purity and high productivity within 30 min. In addition, the pcMNPs showed good binding with viral RNA, resulting in 10-copy sensitivity using the RT-PCR-based detection technique.

2.3. Quantum Dots. Due to their unique optical and electrical properties, QDs have been applied in the detection of several viruses.[53,54] For coronavirus detection, a QD-conjugated RNA aptamer specific to the SARS-CoV *N* protein has been reported to have high sensitivity in recognizing immobilized viral protein on designed chips.[36] The authors used commercially available QD-605 with an emission maximum at 605 nm to obtain an outstanding detection limit for the SARS-CoV *N* protein at 0.1 pg/mL by detecting the fluorescent emission intensity measured by confocal laser scanning microscopy.[36]

The nanohybrid structures of QDs and other NPs have also been reported for coronavirus detection. Because of their extraordinary plasmonic properties, star-shaped chiroplasmonic AuNPs were combined with CdTe QDs to construct a chiral optical biosensor.[37] Two influenza virus antibodies named anti-HA and anti-NA were immobilized on the surfaces of the star-shaped gold NPs and CdTe QDs, respectively. When a recombinant protein of influenza A (H5N1) was present in the same solution containing both anti-HA-conjugated AuNPs and anti-NA-conjugated QDs, AuNP−QD nanohybrids were formed through antigen−antibody interactions (immunolinking) of the recombinant protein with the two antibodies immobilized on the surfaces of the NPs and QDs. The plasmon−exciton interaction in the newly created AuNP−QD nanohybrids significantly enhanced the chiral optical response of the solution. Consequently, the viral recombinant protein was detected based on the measured circular dichroism response of the solution. In this technique, star-shaped AuNPs were chosen due to their broad plasmonic peak at 590 nm that maximizes the optical coupling and overlaps with the QD excitonic wavelength. The method showed sensitivity at 1 pg/mL for H5N1 detection and was able to detect several other viruses in blood samples, such as avian influenza A (H4N6) virus, fowl adenovirus, and coronavirus.[37] In 2018, a similar approach was used by the same research group to develop a magnetoplasmonic−fluorescent biosensor based on zirconium QDs (ZrQDs) and Fe_3O_4@Au core−shell magnetoplasmonic NPs (MPNPs). As shown in Figure 4, two types of particles were functionalized with viral antibodies. The viral antibody-functionalized NPs stayed apart from each other in the solution. After the target virus was added to the system, the conjugated ZrQDs and MPNPs formed magnetoplasmonic−fluorescent nanohybrid structures via immunolinking. Hence, the detection of the target virus was based on the photoluminescence (PL) properties of the ZrQD−Fe_3O_4@Au MPNP nanohybrids after simple magnetic separation. The nanohybrid structures also showed a change in photoluminescence emission intensity with a change in virus concentration in the system.[38] The method can selectively detect the presence of infectious bronchitis virus (IBV) at a concentration of 79.15 EID/50 μL in blood medium.

https://dx.doi.org/10.1021/acsanm.0c01978
ACS Appl. Nano Mater. 2020, 3, 8557−8580

3. NANOPARTICLES FOR THERAPEUTICS

Much is still unknown about SARS-CoV-2, but it has been determined to be an enveloped virus with spike proteins as the main cell-infecting sites and an ssRNA as the genetic material. Many viruses investigated in NP-based antiviral research are from the coronavirus family or share a similar structure with SARS-CoV-2. NP-based therapeutic drugs can inhibit the effects of viral infection in several ways, including by blocking receptor binding and cell entry, blocking viral replication and proliferation, and directly inactivating the virus. These therapeutic strategies are discussed in this section. Table 2 lists the NPs that can be used for therapeutic strategies against coronavirus infections together with the key takeaways that can be applied for COVID-19.

3.1. Nanoparticles That Block Cell Attachment and Viral Entry. Viral infections start with the binding of viral particles to receptors on the host cells, followed by the entry of the virus into the cells. In the case of SARS-CoV-2, the spike *S* glycoprotein is responsible for cell binding and entry.[82,83] As illustrated in Figure 5a, the *S* protein of SARS-CoV-2 can be divided into two subunits: the *S*1 subunit is responsible for attachment, while the *S*2 subunit mediates membrane fusion and entry into the cell.[82,84] The *S*1 subunit consists of an N-terminal domain (NTD) and a C-domain; the *S*2 subunit consists of a potential fusion peptide (pFP), heptad repeats N and C (HR-N, HR-C), and a transmembrane domain (TM). The *S*1 protein has been shown to bind specifically to the human angiotensin-converting enzyme 2 (ACE2) receptor on the surface of human cells.[13,82] Membrane fusion of the attached virus mostly occurs via endocytosis.[13,83] Therefore, blocking the mechanism by which the virus binds to the ACE2 receptor or blocking viral endocytosis is a potent strategy for drug development and treatment. One of the drugs being widely considered for this purpose is chloroquine. Chloroquine has been shown to inhibit endocytosis of NPs in general; since SARS-CoV-2 is morphologically similar to NPs, chloroquine can block the endocytosis of SARS-CoV-2 virus particles as well, as illustrated in Figure 5b.[85] The proposed mechanism involves chloroquine-induced suppression of PICALM, which prevents endocytosis-mediated uptake of NPs, including SARS-CoV-2. Although chloroquine blocks NP endocytosis into the cell, the efficacy of chloroquine depends on its delivery and cellular uptake, which can be greatly aided by encapsulating the molecule inside polymeric NPs. The most commonly used NPs for encapsulating chloroquine are poly(lactic acid) (PLA) polymeric NPs.[80]

In addition to facilitating drug delivery, NPs can also directly interfere with receptor binding and cell entry of viruses. Ting et al. demonstrated that ∼1.6 nm cationic carbon dots (CDs) synthesized from curcumin (CCM-CDs) can block viral entry of porcine epidemic diarrhea virus (PEDV), a coronavirus model.[76] The inhibition efficiency was over 50% at 125 μg/mL, blocking viral entry at an early stage (see Figure 6a). The blocking is most likely caused by electrostatic interactions between the cationic CDs and the negatively charged PEDV, which neutralizes the effective charge on the virus particles, leading to virus aggregation, as seen from the zeta potential data in Figure 6b. The CDs also suppressed the accumulation of reactive oxygen species (ROS), reducing cell apoptosis. Curcumin can also act as a reducing and capping agent in the synthesis of curcumin-modified AgNPs (cAgNPs), which have also been shown to inhibit cell entry of respiratory viruses.[60] For this purpose, smaller cAgNPs with large surface areas are seen to be more effective than larger NPs. Interestingly, smaller cAgNPs are also less cytotoxic than larger NPs.[60] The driving force behind this process is the same as that for "protein corona" formation; high surface areas of small AgNPs lead to direct interactions with the viral envelope proteins and greater inhibition.[60] Graphene QDs have also been found to be effective in interfering with cell binding of HIV,[86] while AgNPs coupled with graphene oxide (GO) sheets have been shown to be effective in blocking cell entry of feline coronavirus (FCoV) and enveloped viruses.[61] Moreover, various surface-functionalized AgNPs and AuNPs have also been shown to be effective in blocking cell entry of HIV and herpes simplex virus (HSV).[87] The advantage of AuNPs is that they are less cytotoxic than AgNPs.[88−90]

In addition to virus aggregation, AuNPs can also directly interfere with the cell entry mechanism, as demonstrated by Huang et al.[59] Similar to the SARS-CoV-2 *S*2 subunit shown in Figure 5a, the *S*2 protein of MERS-CoV contains heptad repeat 1 (HR1), heptad repeat 2 (HR2), and a fusion protein (FP). As illustrated in Figure 7a, after the FP inserts into the cell membrane, HR1 and HR2 bind to form a six-helix bundle (6-HB). The 6-HB pulls together the MERS-CoV envelope and host cell membrane, promoting fusion. Huang et al. identified a peptide, named pregnancy-induced hypertension (PIH), which could mimic the conformation of HR2. Thus, this peptide can interact with HR1 to block the formation of 6-HB, inhibiting the cell fusion process. When PIH was immobilized on the surface of gold nanorods (PIH−AuNRs), a 10-fold higher inhibitory activity was observed that could completely block cell fusion at the optimized concentration (see Figure 7c,d). The PIH−AuNRs also demonstrated excellent biocompatibility (see Figure 7b).

In addition to AuNPs, other NPs have also been shown to be effective at blocking viral entry while maintaining low toxicity. Among synthetic NPs, porous silicon NPs (SiNPs) are especially favored due to their extreme biocompatibility. SiNPs are biodegradable, since they gradually dissolve in water to form nontoxic silicic acid.[66] Osiminka et al. showed that SiNPs were able to act as scavengers of free virus particles and prevented them from infecting host cells. Binding of SiNPs with virions is universal for different enveloped viruses, making them potential agents against SARS-CoV-2 as well.[66] Mesoporous-SiO_2 ($mSiO_2$) NPs, when functionalized with various moieties, exhibit the ability to attach themselves to enveloped viruses via hydrophobic/hydrophilic interactions. Strong bonds between the functionalized $mSiO_2$ NPs and the virus disturb the virus's attachment to host cell receptors and reduce viral entry into the cells.[72] Other types of biocompatible NPs known for inhibiting cellular entry of viruses include selenium NPs (SeNPs). Selenium is biocompatible, being present in several selenoproteins that are crucial for biological processes, and exhibits antiviral effects at high concentrations.[91] The antiviral activity of SeNPs can be further amplified when these NPs are combined with the antiviral drug Arbidol (ARB), effectively blocking cell entry of influenza virus and reducing cell apoptosis. Cationic chitosan, a nontoxic polysaccharide, has also shown the ability to interact with the *S* protein of various human coronaviruses and block their interaction with the ACE2 receptor.[92] Raghuwanshi et al. utilized cationic chitosan NPs functionalized with targeted antibodies for efficient delivery of a vaccine to dendritic cells

https://dx.doi.org/10.1021/acsanm.0c01978
ACS Appl. Nano Mater. 2020, 3, 8557−8580

Table 2. Nanoparticles for Therapeutics

NPs	conjugate	size (nm)	cytotoxicity (dose, time)	virus	approach	level of study	key takeaways for COVID-19	ref.
AuNPs	sialic acid	14	99% cell viability	**IAV**	infection inhibition	in vitro	40% infection reduction	55
	MES	4 ± 1	-	**IAVs**	infection inhibition	in vitro	80% infection reduction	56
	MES/MUS-OT	2.5 ± 0.7	noncytotoxic	**RSV, VSV, HPV, dengue**	viricidal therapy	in vivo/ex vivo	permanent damage of up to 87% virus, no lung damage	57
porous AuNPs	-	154 ± 37	95% cell viability (0.2 mg/mL, 24 h)	**H1N1, H3N2, H9N2**	infection inhibition	in vitro	96.8% survival rate of infected cell	58
AuNRs	PH peptide + PEG	54:18	no cytotoxicity	**MERS**	block viral entry	in vivo	PIH−AuNRs are 10-fold better than PIH; inhibit 90% cell fusion, AuNRs improve biostability	59
AgNPs	curcumin	20	cell viability >95% (0.24 nM, 72 h)	**RSV**	block viral entry	in vitro	cAgNPs directly interfere with virus, curcumin reduces AgNP toxicity	60
	graphene oxide	<10	cell viability >90% (1.5625 mg/mL, 24 h)	**FCoV**	block viral entry	in vitro	graphene oxide becomes effective against enveloped viruses on coupling with AgNPs	61
	-	<20	>80% cells unaffected (12.5 μg/mL, 48 h)	**TGEV-CoV**	replication/infection inhibition	in vitro	67.35% virus reduction	62
	oseltamivir	3	-	**H1N1**	infection & apoptosis inhibition	in vitro	90% infected cell viability	63
	zanamivir	3	-	**H1N1**	infection & apoptosis inhibition	in vitro	82% infected cell viability	64
	-	10	minor mucosal thickening	**RSV**	replication inhibition	in vitro/in vivo	79% replication reduction, no illness in mice	65
SiNPs		5−50	no cytotoxicity	**HIV, RSV**	block viral entry	in vitro	effective against enveloped viruses, biodegradable	66
SeNPs	zanamivir	82	-	**H1N1**	infection inhibition	in vitro	73% infected cell viability	67
	amantadine	70	-	**H1N1**	infection & apoptosis inhibition	in vitro	79% infected cell viability	68
	ribavirin	65	-	**H1N1**	infection & apoptosis inhibition	in vitro/in vivo	81% infected cell viability, lungs protected	69
	oseltamivir	100	-	**H1N1**	infection inhibition	in vitro	93% infected cell viability	70
ZnO NPs	PEG	18	>90% cell viability (0.2 mg/mL, 24 h)	**H1N1**	viral inactivation	in vitro	90% infected cell viability	71
SiO_2NPs	GPTMS, APTES, TMPES	354	65% cell viability (0.1 mg/mL, 48 h)	**HIV, VSV**	infection inhibition	in vitro	50% infection reduction	72
Fe_3O_4@SiO_2	biguanide, polymeric aziridine	150	>80% cell viability (0.2 mg/mL, 5 h)	**HSV**	viral inactivation	in vitro	50-fold antiviral improvement effect on antiviral conjugates	73
Ag_2S	glutathione	4.1 ± 1.5	>90% cell viability (46 μg/mL, 48 h)	**PEDV-CoV model**	replication inhibition/ immunity activation	in vitro	viral titer reduced 1000 times	74
CDs	R-B$(OH)_2$, NH_2	9.2 ± 0.3	nontoxic at 100 μg/mL, 24 h	**HCoV-229E**	block viral entry and viral replication	in vitro	inhibition of cell entry with CDs enhanced by boronic acid	75
	-	1.5	>90% cell viability (125 μg/mL, 48 h)	**PEDV-coronavirus model**	replication inhibition/ immunity activation	in vitro	80% viral reduction	76
	-	11.4	noncytotoxic (0.3 mg/mL, 24 h)	**PRRSV-CoV model**	viral inactivation	in vitro	10-fold viral reduction	77
	-	4.4 ± 0.6	-	**Zika, dengue**	infection inhibition	in vitro	90% infected cell viability	78
cellulose nanocrystals	tyrosine sulfate	113	>80% cell viability (−)	**Alphavirus**	infection inhibition	in vitro	100% infection inhibition	79
PLA NPs	chloroquine	<300	Cell viability ≥70% (30 μg/mL, 48 h)	**HSV-1**	block viral entry	in vitro	slow and targeted release of chloroquine with PLA NPs, which also reduces chloroquine toxicity. PLA is biodegradable	80

https://dx.doi.org/10.1021/acsanm.0c01978
ACS Appl. Nano Mater. 2020, 3, 8557−8580

Table 2. continued

NPs	conjugate	size (nm)	cytotoxicity (dose, time)	virus	approach	level of study	key takeaways for COVID-19	ref.
lipid nanodiscs	sialic acid	15	-	H1N1	viral inactivation	in vitro/in vivo	60% infection reduction, 40% death rate reduction in mice	81

[a]Abbreviations: PLA: poly(lactic) acid, HSV: herpes simplex virus, CDs: carbon dots, RSV: respiratory syncytial virus, FCoV: feline coronavirus, cAgNPs: curcumin-modified Ag nanoparticles, HIV: human immunodeficiency virus, MES: 3-mercaptoethylsulfonate, MUS: undecanesulfonic acid, OT: 1-octanethiol, APTES: (3-aminopropyl)triethoxysilane, GPTMS: (3-glycidyloxypropyl)-trimethoxysilane, TMPES: trimethoxy-(2-phenylethyl)silane, VSV: vesicular stomatitis virus, HPV: human papillomavirus, PEDV: porcine epidemic diarrhea virus, TGEV: transmissible gastroenteritis coronavirus, IAV: influenza A virus.

(DCs) via the intranasal route, but these NPs have potential for use as DC-targeting drugs for blocking viral entry as well.[93]

3.2. Nanoparticles That Block Viral Replication and Proliferation. For viral infection, therapeutics that inhibit the proliferation speed or infectivity of viruses are of paramount importance. These treatments will keep the virus level in the body low enough for the immune system to respond effectively and in a timely manner as the first line of defense as well as to limit the virus's capability to resist treatment via genetic mutation. Due to multiple outbreaks, respiratory diseases caused by members of the coronavirus family have received much research attention over the past decade for the development of effective therapies. Various NPs have been investigated as antiviral agents for inhibition of viral proliferation.

The infectivity of the transmissible gastroenteritis virus (TGEV), a member of the coronavirus family, is significantly diminished in the presence of AgNPs and silver nanowires (AgNWs) at concentrations below the toxic level.[62] Silver nanostructures have also been demonstrated to decrease cell apoptosis induced by viral infection. Data have suggested that Ag nanomaterials regulate p38-MAPK-p53 mitochondrial signaling cascades by inhibiting TGEV-induced expression of the Pi-p38 protein. This regulation reduces cell apoptosis induced by TGEV infection.

PEDV is a commonly studied model virus of the coronavirus family due to its high similarity to other human-infecting coronaviruses and the economic impact caused by PEDV infection. Han and co-workers reported the suppression of PEDV infection by 3 orders of magnitude via treatment with glutathione-capped Ag_2S nanoclusters (Ag_2S NCs).[74] The study also pointed out that the mechanisms of inhibition of viral proliferation are based on the suppression of RNA synthesis, as shown in Figure 8. The authors further found that Ag_2S NCs activated the generation of interferon (IFN)-stimulating genes (ISGs) and cytokine expression, which further inhibited viral infection.

In addition to members of the coronavirus group, there are various viruses with structures similar to that of SARS-CoV-2 with positive-sense ssRNA genetic material, an envelope of phospholipids, and proteins. Many of these viruses have even been used as models for coronavirus research in recent years, and the efficacy of nanoparticles on these viruses could be relevant to therapy development for SARS-CoV-2. As one of the most heavily studied viruses due to multiple global pandemics in the last 100 years, influenza A viruses with their frequent genetic mutation and increasing resistance to drugs have been the target for various NP-based therapeutic research efforts. A potentially effective therapeutic target of many influenza viruses is hemagglutinin (HA), a highly conserved surface protein possessing six disulfide bonds. Haam and co-workers used porous gold NPs (PoGNPs) to target the HA protein on various influenza viruses based on strong gold−thiol interactions.[58] The results demonstrated significant inhibition of viral infectivity in cells treated with PoGNPs, and the cell viability increased to 96.8%, compared to 33.9% of nontreated cells. The viral inhibition efficacy was confirmed on the H1N1, H3N2, and H9N2 viruses to demonstrate the universal effectiveness of the approach. The biocompatibility of PoGNPs was also evaluated by the WST-1 assay, showing 95% cell viability. Alghrair et al. reported that AgNPs and AuNPs functionalized with FluPep, a peptide that can effectively inhibit influenza A viruses (IAVs), showed greater antiviral

https://dx.doi.org/10.1021/acsanm.0c01978
ACS Appl. Nano Mater. 2020, 3, 8557−8580

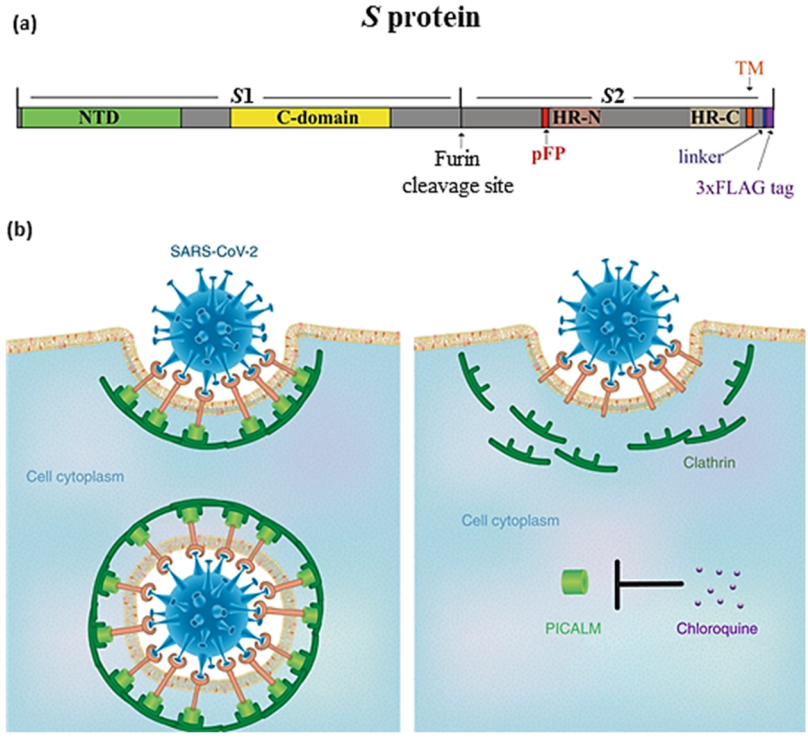

Figure 5. (a) Diagram of full-length SARS-CoV-2 *S* protein with a 3xFLAG tag. *S*1: receptor-binding subunit; *S*2: membrane fusion subunit; TM: transmembrane domain; NTD: N-terminal domain; pFP: potential fusion peptide; HR-N: heptad repeat-N; HR-C: heptad repeat-C. Reproduced with permission from ref 83. Copyright 2020 Springer Nature. (b) Potential mechanism by which chloroquine exerts therapeutic effects against COVID-19. The proposed mechanism involves chloroquine-induced suppression of PICALM, which prevents endocytosis-mediated uptake of nanoparticles, including SARS-CoV-2. Adapted with permission from ref 85. Copyright 2020 Springer Nature.

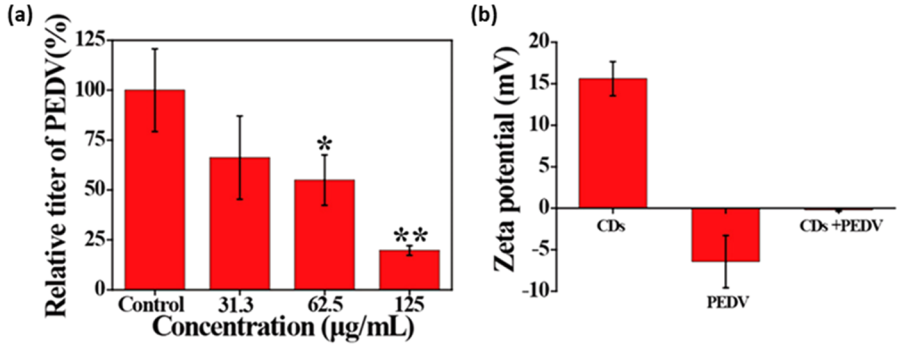

Figure 6. (a) Dose relationship between the viral entry inhibitory efficiency and amount of added CCM-CDs. (b) Zeta potentials of CCM-CDs, PEDV, and CCM-CDs pretreated with PEDV, indicating aggregation of PEDV upon treatment with CDs. Reproduced with permission from ref 76. Copyright 2018 American Chemical Society.

activity than free FluPep.[94] Haag and co-workers used electron microscopy imaging to visually show that AuNPs functionalized with sialic-acid-terminated glycerol dendrons specifically targeted the viral HA protein to effectively inhibit viral proliferation.[55] Moreover, various NPs, such as oseltamivir-functionalized AgNPs,[63] AgNP/chitosan composites,[95] zanamivir-functionalized AgNPs,[64] zanamivir-functionalized SeNPs (through the p38 and JNK signaling pathways),[67] amantadine-functionalized SeNPs (through the ROS-mediated AKT signaling pathways),[68] ribavirin-functionalized SeNPs (via the caspase-3 apoptotic pathway),[69] oseltamivir-functionalized SeNPs,[70] PEGylated-ZnO NPs,[71] and anionic AuNPs,[56] have also been fabricated and investigated for inhibitory effects on and biocompatibility with H1N1, a current seasonal virus that caused two deadly global pandemics in 1918 and 2009.

In addition to influenza viruses, porcine reproductive and respiratory syndrome virus (PRRSV), a model virus often used for coronavirus research, has also been reported to be highly suppressed after exposure to AgNP-modified GO (GO−AgNPs) with 59.2% inhibitory efficiency.[96] GO−AgNP nanocomposite treatment also enhanced the production of IFN-α and ISGs, which can directly inhibit viral proliferation. In another study, Tong et al. reported the synthesis of glycyrrhizic-acid-based CDs (Gly-CDs) and their high inhibitory activity of up to 5 orders of viral titers through multisite inhibition of PRRSV.[77] The multisite viral inhibitory mechanisms of Gly-CDs include inhibition of viral invasion and replication, stimulation of IFN production in cells, and inhibition of viral-infection-induced ROS production, providing a promising alternative for coronavirus infection therapy as

https://dx.doi.org/10.1021/acsanm.0c01978
ACS Appl. Nano Mater. 2020, 3, 8557−8580

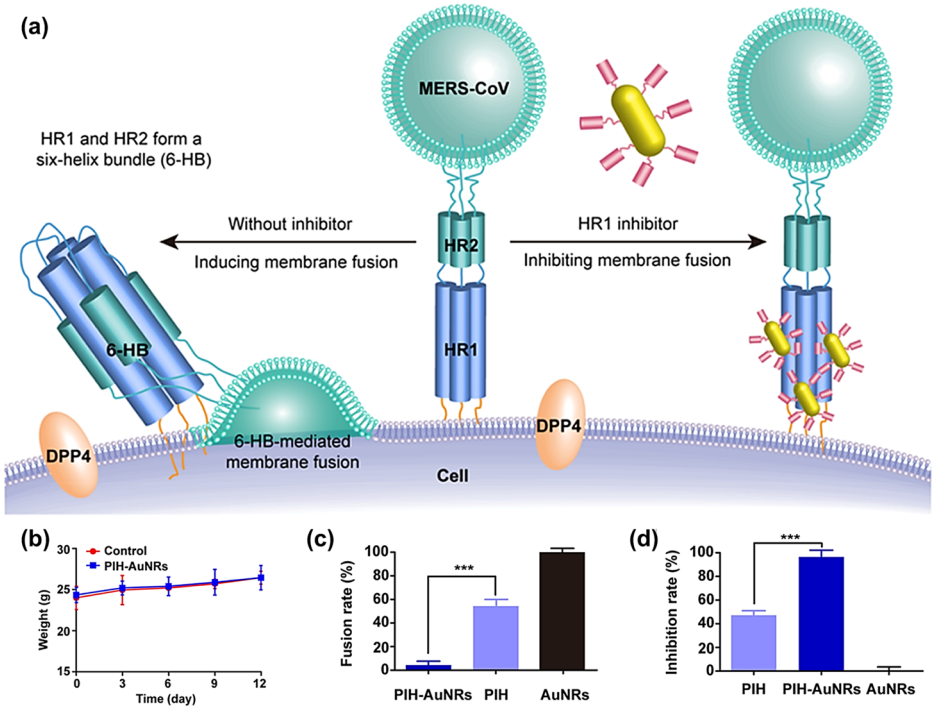

Figure 7. (a) Schematic diagram of the inhibition of MERS-CoV *S*2-subunit-mediated membrane fusion with an HR1 inhibitor (left); the HR1 inhibitor can inhibit HR1/HR2 complex (6-HB)-mediated membrane fusion and prevent MERS-CoV infection (right). (b) Body weights of mice in both the PIH−AuNR group and control group steadily increased, demonstrating excellent biosafety of PIH−AuNRs. (c) Quantification of cell fusion in the presence of PIH, AuNRs, and PIH−AuNRs. (d) Inhibitory effect of PIH−AuNRs on MERS-CoV *S*2-subunit-mediated cell fusion, indicating that PIH−AuNRs are more potent anti-MERS agents than the peptide PIH. Reproduced with permission from ref 59. Copyright 2019 American Chemical Society.

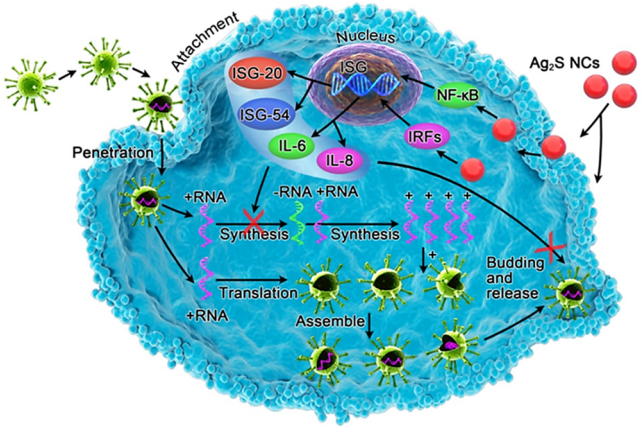

Figure 8. Possible mechanisms of the antiviral activity of Ag_2S NCs via inhibition of the synthesis of viral RNA and viral budding due to the production of ISGs and upregulation of proinflammatory cytokines. Reproduced with permission from ref 74. Copyright 2018 American Chemical Society.

well as PRRSV infection therapy. This work also showed the remarkable ability of Gly-CDs to suppress PEDV and pseudorabies virus (PRV), suggesting a broad antiviral capability compared to previous work.[97] These results on model viruses might serve as guides for research and development on SARS-CoV-2.

The infection caused by Zika virus, a virus with a similar structure to coronaviruses and the cause of a widespread epidemic in South and North America in 2015, was suppressed by benzoxamine-monomer-derived CDs (BZM-CDs).[78] The data from a plaque uniform assay and transmission electron microscopy (TEM) showed that BZM-CDs could reduce viral infectivity via direct interaction with the viruses. The inhibitory ability of BZM-CDs was also demonstrated on Japanese encephalitis and dengue viruses, two other life-threatening viruses that also exhibit structural similarity to coronaviruses, as well as on nonenveloped viruses (e.g., adeno-associated virus (AAV), porcine parvovirus (PPV)), suggesting that the broad-spectrum potential of the NPs should be further investigated for SARS-CoV-2.

Alphaviruses, a genus of RNA viruses with a structure similar to that of coronaviruses, were strongly inhibited in Vero (B) cells by cellulose nanocrystals (CNCs) modified with tyrosine sulfate mimetic ligands, while no observable cytotoxicity in human cells was detected.[79] The incorporation of tyrosine sulfate mimetic ligands on CNCs led to increased viral inhibition compared to incorporation of the control CNCs. This discovery suggests potential applications of CNCs for the treatment of HIV and HPV. In addition, studies of NP-based antiviral treatment of viruses similar to SARS-CoV-2 were also reported for AgNPs with Chikungunya virus (CHIKV) and respiratory virus (RSV),[65,98] cAgNPs with RSV,[99] and SiNPs with RSV.[66]

In the coronavirus family, the outer envelope with the surface proteins is vitally important to the infection and proliferation of the virus. Various studies have reported the remarkable efficacy of NP-based inhibition of HIV by targeting the viral outer envelope using AgNPs,[100] AuNPs,[101−103] porous SiNPs,[66] and silica NPs.[72] Human-related enveloped viruses such as vesicular stomatitis virus (VSV), tacaribe virus, PRV, and HSV have also been shown to be significantly inhibited by silica NPs,[72] AgNPs,[104] CDs,[97] and modified

https://dx.doi.org/10.1021/acsanm.0c01978
ACS Appl. Nano Mater. 2020, 3, 8557−8580

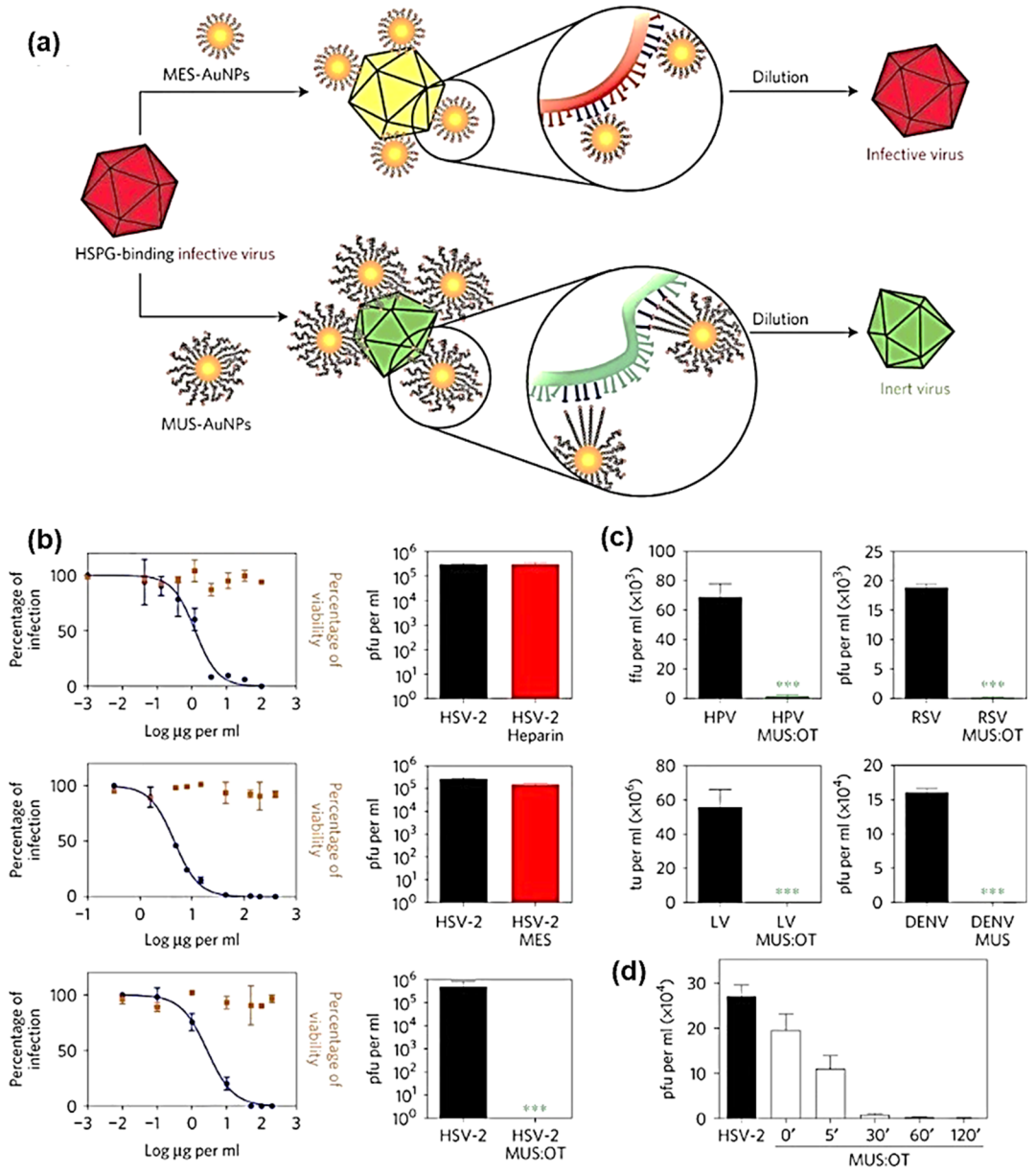

Figure 9. (a) Viricidal activity of AuNPs coated with MES or MUS. (b) Heparin, MES-coated AuNP, and MUS:OT-coated AuNP viral infectivity curves (blue) and viricidal assays at concentrations corresponding to the EC_{90} (black) and after dilution (red). (c) Viricidal activity of MUS:OT-coated AuNPs against HPV, RSV, VSV (indicated as LV), and dengue virus (DENV-2). (d) MUS:OT-coated AuNP-mediated inhibition of viral infectivity against HSV-2 versus time (min). Reproduced and adapted with permission from ref 57. Copyright 2017 Springer Nature.

AgNPs,[105−107] respectively. These NP-based antiviral therapies targeting the outer envelopes of enveloped viruses are very relevant to further studies on SARS-CoV-2.

3.3. Nanoparticles for Viral Inactivation and Viricidal Treatment. Instead of inhibiting the cell−virion interaction, genetic material replication, or release of newly formed virions, another strategy to halt viral infection is inactivation or destruction of the virus itself. In an elegant study led by Stellacci, AuNPs coated with 3-mercaptoethylsulfonate (MES) showed viral infection inhibition at a concentration corresponding to the EC_{90}, but the viral infectivity was fully recovered upon dilution. This process is called reversible viral inhibition and is similar to the effect of heparin, a common virustatic material that targets virus−cell interactions. Interestingly, the authors found that when MES was substituted by a 2:1 mixture of undecanesulfonic acid (MUS) and 1-octanethiol (OT), the MUS:OT−AuNPs could induce irreversible viral inactivation of various human-infecting viruses, ranging from HSV, VSV, RSV, and dengue virus to HPV and lentivirus.[57] The MUS ligand has a long and flexible hydrophobic backbone terminated with sulfonic acid mimicking the heparin sulfate proteoglycan (HSPG), a common and highly conserved target of viral attachment ligands, allowing effective virus−NP binding. This strong binding force (∼190 pN) led to irreversible deformation of the virus, as shown in Figure 9. The strong viral−MUS:OT−AuNP binding was further confirmed by electron microscopy imaging and molecular dynamics simulation. Moreover, an in vivo test in mice and an ex vivo test in human cervicovaginal histocultures also demonstrated the viral inactivation activity of the MUS:OT−AuNPs, with no cytotoxicity observed. This strategy is intrinsically broad spectrum, allowing viricidal treatment of

https://dx.doi.org/10.1021/acsanm.0c01978
ACS Appl. Nano Mater. 2020, 3, 8557−8580

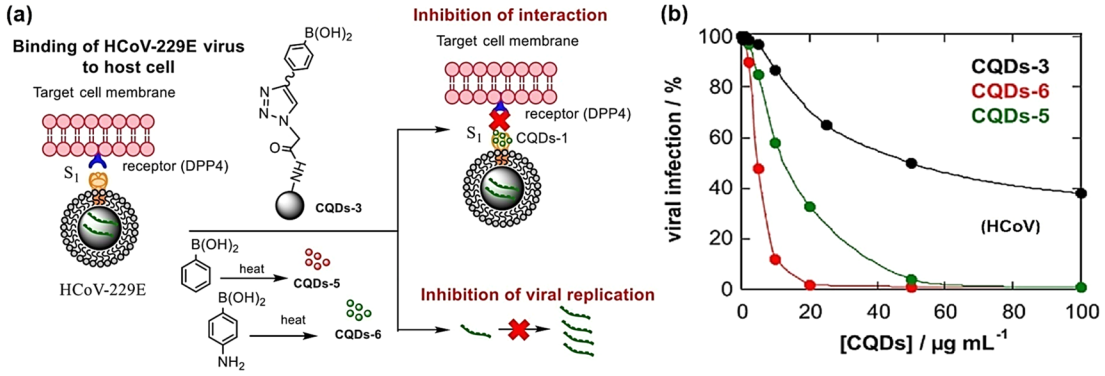

Figure 10. (a) Effect of CQD on HCoV by inhibition of *S* protein−receptor interaction (top) and viral RNA genome replication (bottom). (b) Viral inhibition using CQDs-3, CQDs-5, and CQDs-6. Reproduced and adapted with permission from ref 75. Copyright 2019 American Chemical Society.

multiple viruses. The viruses used in the study were very similar to coronaviruses, suggesting the potential applicability of the method for SARS-CoV-2.

In another study, Kong et al. showed that decoy virus receptor-functionalized nanodiscs, self-assembled discoidal phospholipid bilayers wrapped in amphipathic membrane scaffold proteins, can inactivate the H1N1 virus by selectively targeting the virion's surface proteins to cause irreversible physical damage to the envelope.[81] The antiviral activity of the viral decoy molecule sialic acid was amplified after grafting onto the nanodiscs due to the enabling of multivalent interactions with viral target proteins. The data also showed that the presence of the functionalized nanodiscs led the virus to self-disrupt its envelope with its own fusion machinery. The strength of this method is the use of biocompatible NPs and viral decoy molecules, making it a compelling method for in vivo studies. Gao and co-workers recently showed the catalytic inactivation of iron oxide (Fe_3O_4) NPs targeting the viral envelopes on 12 different subtypes (H1−H12) of IAVs.[108] The ferromagnetic Fe_3O_4 NPs with an average diameter of 200 nm were named iron oxide nanozymes (IONzymes) due to their unique enzyme-like property, catalyzing peroxidase and catalase reactions. Consequently, IONzymes could strongly induce lipid peroxidation in the viral envelope and destroy the integrity of viral surface proteins, including HA, neuraminidase, and matrix protein I, leading to inactivation of the viruses. Additionally, the authors loaded the IONzymes on facemasks and observed good protection against multiple strains of IAVs, including H1N1, H5N1, and H7N9. The biocompatibility and simple synthesis of the IONzyme nanomaterial make it attractive for effective and safe early stage antiviral therapeutics. Thus, the IONzyme nanomaterials present a potentially powerful approach against SARS-CoV-2.

In addition to the works highlighted above, other studies also reported promising inactivation and viricidal effects of different NPs on many viruses that share structural similarities with SARS-CoV-2. Among those reports are the inhibition of dengue virus by photosensitizer-carrying upconversion NPs, which can convert low-energy photons to high-energy photons;[109] inhibition of the measles virus by AuNPs synthesized by using *Allium sativa* (garlic extract) as a reducing agent;[110] inhibition of hepatitis C virus by AuNP-based nanozymes;[111] inhibition of HSV by poly(hexamethylene biguanide) (PHMBG) or aziridine-terminated polyethylenimine-functionalized superparamagnetic iron oxide@silica core−shell NPs;[73] inhibition of IAVs by AgNP-decorated silica particles;[112] inhibition of H1N1 virus by didodecyldimethylammonium bromide-coated silica NPs,[113] HIV by AgNPs;[114] peptide triazole Env inhibitor-conjugated AuNPs;[103] and T-cell-mimicking NPs based on poly(DL-lactide-coglycolide) NP cores.[115]

3.4. Nanoparticles Combining Multiple Approaches for Treatment. In addition to NPs that employ one of the three methods mentioned above to treat viral infection, various works have also shown NPs that can attack viruses via a combination of approaches. Nanoparticles that can inhibit the viruses via multiple mechanisms offer more effective opportunities for reducing viral infection through synergetic effects. Recently, Szunerits and co-workers modified carbon QDs (CQDs) of different sizes in the range of 4.5−8 nm with various functional groups, including NH_2, COO^-, N_3, triazole, R-$B(OH)_2$, and PEG, for human coronavirus (HCoV) therapy.[75] Biocompatible QCDs functionalized with triazole, boronic acid, and amino groups showed significant inhibition of HCoV infection in a concentration-correlated manner. Mechanistic studies by the authors suggested that the particles not only interfere with the replication of HCoV but also inhibit the interaction of the surface *S* protein with the host cell and therefore interrupt the cell fusion of HCoV as shown in Figure 10. Rather than interacting with viral proteins, these CDs interfere with the cellular mechanism for *S* protein attachment and viral uptake. This work demonstrated highly promising antiviral agents based on biocompatible NPs, which should be further investigated for their activity against SARS-CoV-2, which is also an HCoV with the *S* protein as the main cell-infecting site.

PRRSV, a model virus for coronavirus studies, has been shown to be directly inactivated and entry-blocked by glutathione-stabilized fluorescent gold nanoclusters (AuNCs).[116] Immunofluorescence assay, Western blot assay, plaque assay, and RT-qPCR assay data indicated that viral proliferation and protein expression were inhibited by AuNCs. The functionalized AuNCs in this study showed low biocompatibility and therefore may not be suitable for in vivo application. However, the coupling of AuNCs with other suitable biocompatible virus-targeting agents could lead to effective virus inactivation.

https://dx.doi.org/10.1021/acsanm.0c01978
ACS Appl. Nano Mater. 2020, 3, 8557−8580

Table 3. Nanoparticles as Immunogenic Agents for Vaccines

NPs	conjugate/ adjuvant	size (nm)	virus	level of study	approach and result	key takeaways for COVID-19	ref
AuNPs	SARS-CoV *S* protein	40, 100	**SARS**	in vivo; BALB/c mice	induce strong IgG response	viral proteins form corona around AuNPs	121
VLPs with AuNPs	avian IBV *S* protein	AuNPs: 100 VLPs: 139	**IBV**	in vivo; BALB/c mice	VLPs with AuNPs induce strong antigen-specific cellular immunity, IgG, IgA responses and reduced symptoms	VLPs with AuNPs retain 200−250 spike proteins for 7 days. virus-like zeta potential, lymphatic antigen delivery 6-fold better with AuNPs	122
VLPs from MERS-CoV *S* protein (full)	alum, Matrix M1	-	**MERS**	in vivo; BALB/c mice	VLPs with Matrix M1 adjuvant induce high anti-S titers	completely blocks MERS-CoV replication in lungs	123
VLPs from SARS-CoV& MERS-CoVSprotein (full)	alum, Matrix M1	~25	**SARS, MERS**	in vivo; BALB/c mice	high antibody titers against homologous virus. virus-specific vaccine	Matrix M1 a powerful adjuvant, better than alum	9
VLPs from MERS-CoVSprotein	Ad5/MERS, alum	VLPs: 35; with alum: 80	**MERS**	in vivo; BALB/c mice	$CD8^+$ T cell response; TNF-a, IL-2, GM-CSF, and IFN-c responses; higher with Ad5/MERS	balanced Th1/Th2 activation generates a longer-lasting antibody response	11
VLPs from proteins and HRC subunit of SARS-CoV-*S*protein		25−30	**SARS**	in vivo; BALB/c mice	nanometer size and epitope display generate neutralizing mice antisera	conformation-specific and repetitive display of epitopes fully protect mice, even in absence of any adjuvant	124
VLPs from bacteriophage P22	IAV HAs	~26	**SARS, Influenza A**	in vivo; C57BL/6 mice	intratracheal. recognizable by TLR-2 receptor. protect from infection and weight loss	repetitive HA epitope acts as self-adjuvant, formation of iBALT, protect mice from lethal doses of SARS-CoV	8
VLPs using canine parvovirus	MERS-CoV RBD, poly(I:C)	~25	**MERS**	in vivo; BALB/c mice	mixed Th1 and Th2 responses. 1:320 increase in antibody titers	parvovirus-like VLPs do not cause disease in humans, safe platform, significant enhancement with poly(I:C) adjuvant	125
chitosan NPs	SARS-CoV *N* protein	210 ± 60	**SARS**	in vivo; BALB/c mice	intranasal, intramuscular. dendritic cell targeting. strong $CD4^+$ response. high levels of IgG, IgG1, IgG2a, IgG2b, IgA, IFN-γ	cationic chitosan easily bind to DNA, better delivery than naked DNA, *N* protein better for broad-spectrum vaccines, mucosal pathway mimic infection route and DC targeted delivery, induce stronger antibody response	93
heat shock protein cage NPs		120	**SARS, H1N1, RSV**	in vivo; C57BL/6, BALB/c, μMT, C3H/HeJ, B6.SJL-Ptprca, Pep3b/BoyAiTac mice	mucosal delivery, induce strong nasal antibodies. formation of iBALT structures of B cells, CD4+ T cells, dendritic cells, and CD8+ T cells. minimal weight loss	broad-spectrum respiratory vaccine, fully protect mice against lethal doses. iBALT structures cause no inflammatory damage to lungs	126
PLGA	STING, MERS-CoV *S* protein, MF59	~148	**MERS**	in vivo; C57BL/6 mice	STING encapsulated in PLGA induce strong RBD-specific $CD4^+$, $CD8^+$, balanced Th1/Th2 response. IgG2a; IFN-β, TNF-α, IL6 generation	polymer NPs for antigen + adjuvant delivery and cellular release, preferentially target lymphatic system	127
CDs		1.6	**PEDV**	in vitro; Vero & PK-15 cells	induce IFNs and proinflammatory cytokines	CDs can trigger innate immune responses	76

[a]Abbreviations: GM-CSF: granulocyte−macrophage colony-stimulating factor, HA: hemagglutinin, iBALT: inducible bronchus-associated lymphoid tissue, PLGA: poly(lactic-*co*-glycolic acid), STING: stimulator of interferon genes.

https://dx.doi.org/10.1021/acsanm.0c01978
ACS Appl. Nano Mater. 2020, 3, 8557−8580

4. NANOPARTICLES AS IMMUNOGENIC AGENTS FOR VACCINES

The most effective way to fight a viral epidemic is through vaccination. The goal of vaccination is to initiate a strong immune response that leads to the development of lasting and protective immunity against the targeted pathogen. The components of the immune system can be broadly classified into two categories: innate (nonspecific) and adaptive (specific) immune systems.[117,118] The innate immune system comprises natural killer (NK) cells, DCs, macrophages, monocytes, and innate lymphoid cells. NK cells eliminate infected cells; macrophages secrete cytokines and chemokines that induce inflammation for local defense or to facilitate tissue repair; DCs act as sentinels, carrying pathogens to adaptive immune cells; monocytes replenish macrophages and DCs; and innate lymphoid cells integrate and amplify cytokines. The adaptive immune system comprises antibodies, B cells, antigen-presenting cells (APCs), T cells, and T-helper (Th) cells. Antibodies are immunoglobins (Igs: IgA, IgD, IgE, IgE, IgG, and IgM), which are the first line of defense, secreted by B cells residing in lymph nodes, after recognition of an antigen, while T-helper (Th) cells assist Ig class switching. IgG and IgA are the two major types of antibodies secreted for direct neutralization of pathogens. The most important T cells are $CD4^+$ and $CD8^+$ T cells, which are the central coordinators of the immune response. $CD4^+$ T cells recognize antigen peptides presented on APCs, while activated $CD8^+$ T cells induce the death of infected cells. Activated $CD4^+$ T cells, called Th1 cells, also produce IFN-γ, which drives the presentation pathway, facilitating recognition, generation of antiviral antibodies by B cells, and killing and disposal of infected cells with the help of NK cells and macrophages. Th cells and macrophages also produce interleukins (ILs) and tumor necrosis factor-α (TNF-α), two important classes of cytokines for antiviral immune responses.[119,120] Table 3 lists the NPs that can be used to trigger innate and adaptive immune responses against coronavirus infections. The most common NP-based vaccines are virus-like particles (VLPs) comprised of viral proteins, while NPs have also been used as vehicles for targeted RNA delivery to components of the innate immune system. The various NP-based vaccine designs are discussed in detail in the following sections.

4.1. Virus-Like Particles. The goal of vaccination is to deliver antigens that activate the immune system against the virus. There are various ways to generate effective vaccines. Currently, most vaccines are based on whole viruses, either live attenuated viruses or inactivated viruses.[128] However, live vaccines are unstable and difficult to deliver, and the potential for genetic reversion to a more virulent form is always a concern. On the other hand, inactivated vaccines induce a weaker immune response. In both cases, ensuring complete inactivation, the absence of any further infection, and full compliance with safety standards takes 12−18 months. This timeline is far from ideal when fighting extremely virulent diseases such as COVID-19. The alternative is to design subunit vaccines that can prime immune responses via delivery of a subset of the viral proteins. Since these vaccines have no potential for replication, subunit vaccines offer a much safer approach and can often be approved faster. Such vaccines can be enabled by using VLPs, which are protein-based NPs containing viral envelope proteins without the accompanying genetic material. Due to their particulate nature, VLPs can mimic whole viruses and are much more stable than soluble antigens. Several VLP vaccines have been licensed for clinical use against various pathogens, such as hepatitis B virus (HBV), HPV, Norwalk virus, HSV, and malaria. Early VLP designs possessed limited immunogenicity due to the absence of *S* epitopes on the surface of the VLPs.[129] Incorporating *S* epitopes in later designs yielded more immunogenic VLPs.

Coleman et al. recently developed MERS-CoV spike (*S*) protein NPs that can protect mice from MERS-CoV infection.[123] The spike (*S*) protein, primarily responsible for receptor binding and cell entry, also induces neutralizing antibodies, making the *S* protein an ideal target for the anti-MERS vaccine. This vaccine also stops MERS-CoV replication in the lungs. In a related study, the same research group used full-length MERS-CoV and SARS-CoV *S* proteins to generate ∼25 nm diameter VLPs consisting of multiple *S* protein molecules.[9] Inoculation with these VLPs leads to the generation of neutralizing antibodies in mice. In both of these studies, neutralizing antibody levels were significantly boosted when the VLPs were used with alum and Matrix M1 adjuvants (15-fold with alum and 68-fold with Matrix M1), as seen in Figure 11a.[9,123] Alum is an aluminum salt that acts as a mild irritant, stimulating inflammasome responses, while Matrix M1 is a saponin-based adjuvant manufactured by Novavax, AB.[9] Novavax is currently developing COVID-19 vaccines using VLPs with full-length glycoproteins adjuvanted with Matrix M1.[118,123,130] Jung et al. also used MERS-CoV spike protein NPs with alum to induce specific IgG antibodies in mice.[11] The spike protein NPs had a diameter of 35 nm, which increased to 80 nm when the NPs were formulated with alum. When used in conjunction with a recombinant adenovirus serotype 5 encoding the MERS-CoV spike gene (Ad5/MERS), Th1/Th2 activation was balanced, generating a longer-lasting antibody response. Figure 11b shows the effectivity of this VLP in MERS-infected mice. The self-assembly of MERS-CoV protein NPs can be further assisted by a ferritin template to ensure the display of target antigens on the surface.[131] Since the spike *S* protein of coronaviruses is the most important antigenic determinant for inducing neutralizing antibodies, repetitive display of these *S* protein epitopes on the surface of the VLPs stimulates a stronger immune response. Pimental et al. observed that even using a smaller segment of the *S* protein may be sufficient if the epitopes are concentrated on the surface.[124] Using template-based synthesis with coiled-coil proteins, the C-terminal heptad repeat region (HRC), and a small segment of the *S* protein, they generated VLPs (see Figure 11c) that were able to stimulate anti-SARS antibodies even in the absence of an adjuvant, attributed largely to its nanometer size, repetitive display of the epitope, and good mimicry of the epitope's natural configuration. Similar results were also observed by Sharma et al. when they incorporated multiple copies of the HA protein on the surface of the VLPs; HA is a surface-exposed glycoprotein and is the most highly immunogenic target for IAV. Immunization of IAV-infected mice with HA-conjugated surface VLPs provided full protection from morbidity and mortality without the need for additional adjuvants.[8] Thus, we observed that VLPs based on the spike *S* protein of MERS-CoV and SARS-CoV were effective in stimulating a strong antibody response. The antibody response is enhanced in the presence of adjuvants or by concentrating multiple repeating units of the *S* protein on the surface of the VLPs.

https://dx.doi.org/10.1021/acsanm.0c01978
ACS Appl. Nano Mater. 2020, 3, 8557−8580

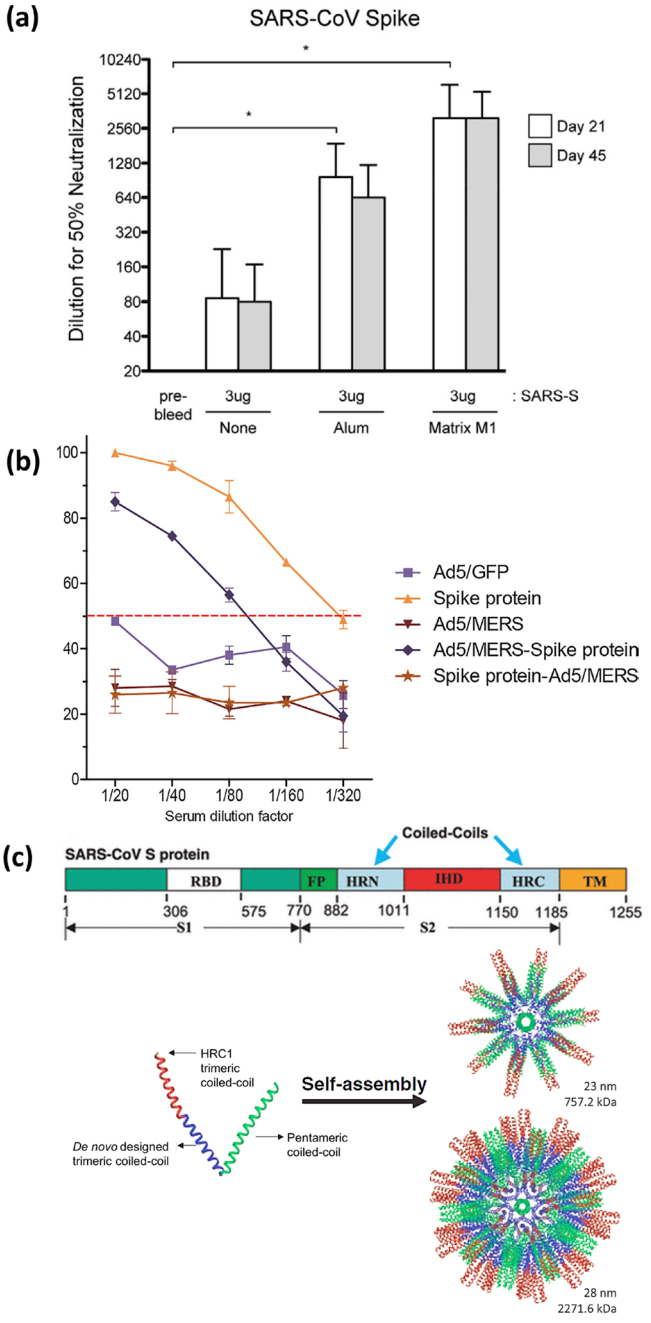

Figure 11. (a) Neutralization titers of coronavirus-spike-vaccinated mice. Serum from mice vaccinated with the indicated mix of spike protein and adjuvant was analyzed for neutralization capability and geometric mean titer (GMT), as graphed for all groups (10 mice per group). Stars denote statistically significant differences ($p < 0.05$). Reproduced with permission from ref 9. Copyright 2014 Elsevier. (b) Titers of neutralizing serum antibody against MERS-CoV in immunized mice. The rate of virus reduction for each group was calculated by comparison with the number of plaques in the control group (with PBS). The red dotted line indicates a 50% reduction in the virus. The mean reduction ± standard deviation values are shown. Reproduced with permission from ref 11. Copyright 2018 Elsevier. (c) Synthetic scheme and computer models for the formation of coiled-coil template-based complete peptide nanoparticles using the HRC region of the S epitope. The inset shows the various segments of the SARS-CoV *S* protein. Reproduced with permission from ref 124. Copyright 2009 Wiley.

Wang et al. designed novel chimeric VLPs using a canine parvovirus structural protein with the receptor-binding domain (RBD) of MERS-CoV.[125] Parvovirus-like particles are very stable, highly immunogenic, and do not cause disease in humans, making them a safe expression platform, while the RBD unit of MERS-CoV is a major antigenic determinant for antibody induction. RBD-specific humoral antibody responses were detected in mice treated with these VLPs 2 weeks after injection and were significantly enhanced in the presence of a polyriboinosinic acid [poly(I:C)] adjuvant. The VLPs produced a Th1-based response with significant IL-2 secretion, while the VLPs with poly(I:C) adjuvant produced mixed Th1 and Th2 responses, producing IFN-γ, IL-2, and IL-4 responses. The IgG antibody titer in mice treated with VLPs along with the adjuvant showed a 320-fold increase in mouse sera. The poly(I:C) adjuvant is able to activate a relatively high number of DCs in lymph nodes to generate a robust immune response. Cross-virus VLP design was also studied by Carter et al.[132] SARS-CoV polyprotein 1a (pp1a) self-assembled into VLPs that were found to be effective against idiopathic pulmonary fibrosis (IPF) caused by *Herpesvirus saimiri* (HVS). These two studies show that VLPs developed using subunits from one virus can serve as effective vaccines against other viruses as well. ARTES Biotechnology has utilized duck hepatitis B small surface antigen to design an enveloped VLP (eVLP) technology called METAVAX to deliver SARS-CoV-2 spike *S* protein-loaded vaccines. ARTES Biotechnology is also utilizing another vaccine technology using capsid VLPs (cVLPs), called SplitCore, to develop vaccines using SARS-CoV-2 *S* antigens. Ufovax, a spin-off vaccine company from Scripps Research, is also developing COVID-19 vaccines using self-assembling protein VLPs (1c-SApNP technology). Similar COVID-19 vaccines with VLPs are also being developed by Medicago (plant-derived VLPs), iBio, Inc. (SARS-CoV-2 VLPs), ExpreS2ion (protein subunit VLPs), GeoVax Laboratories (GV-MVA-VLP), BIKEN (protein subunit VLPs), Saiba GmbH (RBD-based VLPs), Imophoron Ltd. (ADDomer), LakePharma (protein subunit NPs), and VBI Vaccine Inc. (enveloped VLPs); most of these vaccines are already in either in the preclinical or clinical trial phase.[130]

4.2. Chitosan, Protein Cage, and Polymer Nanoparticles for Targeted Vaccine Delivery. NPs have been widely explored for drug delivery applications due to their favorable size, photothermal and magnetic properties, controlled release, and easy functionalization, enabling targeted attachment to specific cell types.[133−137] Many researchers have also attempted to utilize these attributes for targeted vaccine delivery to cellular components of the immune system. DCs are special sentinel cells, a type of APCs. Various strategies employed for selective targeting of DCs have shown great potential in the design of low-dose vaccines.[138] Raghuwanshi et al. designed a vaccine targeting DCs using chitosan NPs as delivery vehicles.[93] Chitosan is a natural polysaccharide that binds strongly to nucleic acids due to its cationic charge,[139,140] which makes these NPs ideal nucleic acid delivery vehicles, further aided by their excellent biocompatible, biodegradable, and nontoxic nature. Raghuwanshi et al. formulated NPs by loading negatively charged plasmid DNA encoding nucleocapsid (*N*) protein as a SARS-CoV vaccine antigen on cationic biotinylated chitosan NPs. Compared to the *S* protein, the *N* protein is more highly conserved in coronaviruses, which offers the ability to design broad-spectrum effectiveness across various mutating strands of the *Coronaviridae* family. For

https://dx.doi.org/10.1021/acsanm.0c01978
ACS Appl. Nano Mater. 2020, 3, 8557−8580

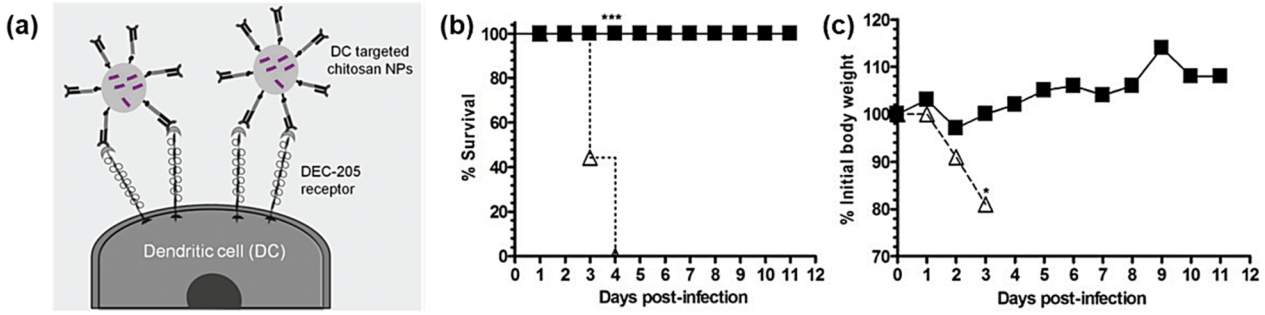

Figure 12. (a) Schematic illustration of dendritic cells targeting chitosan nanoparticles loaded with *N* proteins. Reproduced with permission from ref 93. Copyright 2012 American Chemical Society. (b) Survival of iBALT-induced PCN- and PBS-treated mice following challenge with SARS-coronavirus. All PCN-treated mice (■) survived infection with SARS-CoV, whereas all of the PBS-treated control mice (Δ) were dead by day 4 postinfection. (c) PCN-treated mice (■) maintained their bodyweight following SARS-CoV infection, whereas PBS-treated control mice (Δ) lost significant amounts of body weight shortly after infection. Reproduced with permission from ref 126. Copyright 2009 Wiley et al.

example, compared to the *S* gene in SARS-CoV-2, which is divergent (>25%) when compared to all other previously described SARS-related coronaviruses, the other three structural proteins are more highly conserved than the spike protein and are necessary for general coronavirus function.[12]

Additionally, similar to SARS-CoV and MERS-CoV, SARS-CoV-2 also primarily attacks the respiratory system, causing acute respiratory distress and pulmonary damage.[10,12,141,142] For this reason, Raghuwanshi et al. specifically administered the *N* protein-loaded chitosan NP vaccine intranasally, targeting the mucosal pathway, mimicking the route of an actual viral infection,[93] which induces both humoral and cellular immune responses. Naked DNA is ineffective in crossing mucosal barriers and is rapidly degraded by nucleases, while chitosan NPs transiently open the tight junctions to allow increased transport across the nasal mucosa. As a result, significant *N* protein-specific IgG, IgG1, IgG2a, and IgG2b antibodies, as well as IFN-γ and Th1 cytokine responses, were stimulated. Compared to systemic vaccination, mucosal vaccination is often more effective against mucosal pathogens due to the ability of these pathogens to induce secretory nasal antibodies.[93,126] Wiley et al. designed a safe broad-spectrum vaccine against multiple coronaviruses using a protein cage NP (PCN) that targets mucosal cells.[126] The PCN does not contain any antigen-specific proteins but is derived from a small heat shock protein (sHsp 16.5) instead, which causes the formation of inducible bronchus-associated lymphoid tissue (iBALT). The iBALT strategy provides an alternative approach for broad-spectrum viral protection in the lungs. The PCN-induced iBALT structures contain B cells, $CD4^+$ T cells, DCs, and $CD8^+$ T cells. $CD4^+$ and $CD8^+$ T cells accumulated rapidly in the lungs of PCN-treated mice. These iBALT responses protected the mice from lethal doses of various respiratory viruses (H1N1, SARS, RSV). Protection against SARS-CoV was already apparent within 3 days after infection, implying that innate mechanisms are also modulated by this PCN treatment (see Figure 12b). Despite the strong antiviral response, no histological damage was observed in the alveolar architecture of the lungs, and eosinophilic influx into the lungs was reduced. Thus, this PCN vaccination targeting iBALT microstructures can nonspecifically enhance immune protection against a diversity of respiratory viruses and in the absence of pulmonary inflammation, thus effectively protecting the host (see Figure 12c).

For cell-specific targeted vaccination strategies, NPs with dimensions of ∼100 nm have been generally found to be good for cellular uptake by DCs via phagocytosis, since they resemble the natural targets for DCs, such as viruses or bacteria.[118] Several studies have found that the submicron size is optimal for mucosal cell uptake and that NPs less than 200 nm in size are more readily transported by draining lymph nodes.[140] NPs with sizes of 20−200 nm have long circulation times and become enriched in lymph nodes, leading to enhanced lymphatic transport, allowing direct access to lymphoid-node-resistant DCs.[118] This feature enhances antigen uptake and presentation to B cells, enhancing the humoral response, or to T cells, allowing immunomodulation.[118] Cationic NPs have been widely used to deliver small interfering RNA (siRNA) to the lungs for the treatment of various respiratory diseases over the years via intranasal and intratracheal routes.[143] To combat a rapidly spreading virus such as SARS-CoV-2, mRNA (mRNA)-based vaccines are promising candidates, since they can be scaled rapidly. Cationic lipid NPs encapsulating mRNA are being widely explored for the development of COVID-19 vaccines.[144] Lipid NPs (LNPs) can deliver mRNA to the cytoplasm, where the mRNA can undergo direct translation to the target protein; this process can then trigger APCs and activation of B cells and T cells.[144] A vaccine developed by Moderna in collaboration with NIAID, containing mRNA encapsulated inside lipid NPs, is currently in phase-2 human clinical trials.[130,145] Moderna's previous MERS and SARS vaccines developed using a similar design had demonstrated 90% reduction in viral load.[145] In addition, vaccines by BioNTech/Pfizer/Fosun Pharma (LNP−mRNA) are also in phase-1/2 trials, while Translate Bio/Sanofi Pasteur (LNP−mRNA), CanSino Biologics/Precision NanoSystems (LNP−mRNA), Daiichi-Sankyo (LNP−mRNA), BioPharma (mRNA VLPs), and RNACure Biopharma (LNP-encapsulated mRNA VLPs) are also developing lipid NP-encapsulated mRNA vaccines, currently in preclinical trials.[130]

Another type of NP used to deliver genetic materials to the lungs via nasal instillation is calcium phosphate (CaP).[146] Since CaP is a naturally occurring substance in mammalian hard tissues, it is a safe and biocompatible biomedical carrier. Additionally, acting as a mucosal adjuvant, CaP can initiate an immune response stronger than that induced by aluminum salts and for longer durations.[129] CaP is often encapsulated with polymers such as poly(lactic-coglycolic acid) (PLGA) and polyethylenimine (PEI), to increase cellular uptake.[146] PEI is known for facilitating targeted delivery and stimulating immune responses in alveolar cells and macrophages, along with other polymeric derivatives of PLGA, such as poly(DL-

https://dx.doi.org/10.1021/acsanm.0c01978
ACS Appl. Nano Mater. 2020, 3, 8557−8580

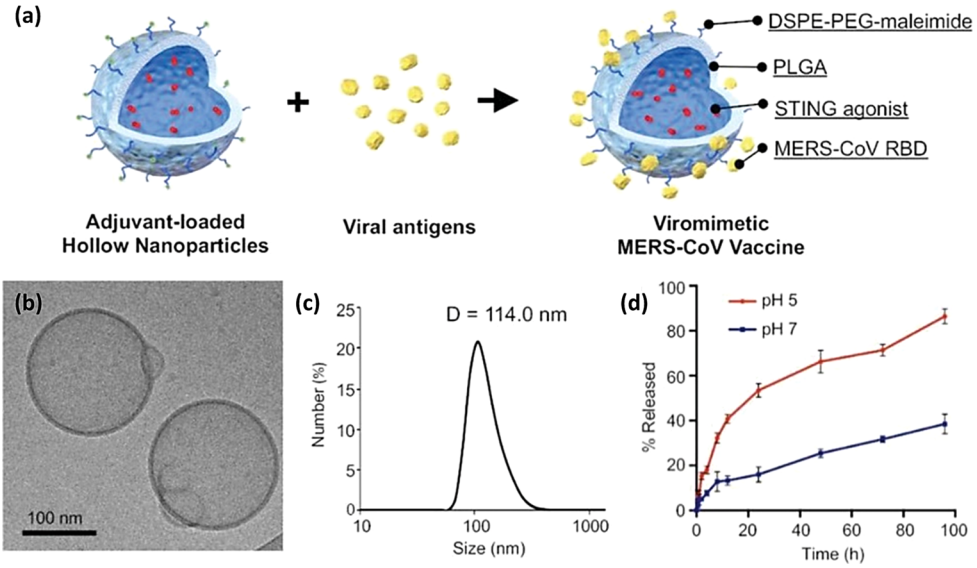

Figure 13. Characterization of adjuvant-loaded viromimetic nanoparticles. (a) Schematic showing the preparation of the viromimetic nanoparticle vaccine. Hollow PLGA nanoparticles with encapsulated adjuvant and surface maleimide linkers were prepared using a double-emulsion technique. Recombinant viral antigens were then conjugated to the surface of nanoparticles via a thiol−maleimide linkage. (b) Cryo-electron microscopy of cdGMP-loaded hollow nanoparticles. (c) Size distribution of nanoparticles determined by dynamic light scattering (DLS). (d) In vitro release profiles of cdGMP from PLGA hollow nanoparticles at pH 5 and 7. Reproduced with permission from ref 127. Copyright 2019 WILEY-VCH Verlag GmbH & Co., KGaA, Weinheim.

lactide-coglycolide) (PLG) and polylactide (PLA).[129,146] Due to their biocompatibility and excellent safety profile, PLGA and PLA have already been approved by the FDA to be used in various drug delivery systems for humans.[80,140] Using a thin (sub-20 nm) shell of PLGA with a large aqueous core, Lin et al. made a hollow NP to entrap a soluble stimulator of IFN genes (STING) adjuvant (see Figure 13).[127] Due to the acid-sensitive PLGA hydrolysis, the NPs readily release the adjuvant upon cellular uptake, as seen in Figure 13. Localized at the endoplasmic reticulum, STING is a potent inducer of proinflammatory cytokines such as IFN-β, TNF-α, and IL-6. When combined with the MERS-CoV spike protein, the STING-PLGA NP size increases to ∼148 nm, which leads to a virus-like distribution of the NPs, synchronizing lymph node delivery of surface-coated antigens and interiorly loaded adjuvant. Further conjugation with the state-of-the-art influenza adjuvant MF59 (Addavax) induced significantly higher levels of antigen-specific antibodies due to balanced Th1 and Th2 responses. Higher antibody titers and longer-lasting responses due to a balanced Th1/Th2 response were also observed by Jung et al., as described previosuly.[11] The polymer-based NPs with STING and MF59 adjuvants were superior in their ability to mount humoral responses compared to free STING agonists or MF59 alone. This study strongly demonstrated the advantages of hollow polymeric NPs as vaccine delivery vehicles due to their biocompatibility, size consistency, colloidal stability, tunable adjuvant loading, pH-responsive release, and antigen functionalizability.

4.3. Quantum Dots and Gold Nanoparticles. QDs, with sizes much smaller than the aforementioned NPs, have also been utilized for designing vaccines against coronaviruses. Positively charged carbon QDs with dimensions of ∼1.6 nm, made from curcumin, were studied as vaccines against PEDV, a model coronavirus.[76] Although these CDs primarily blocked viral cell entry, they also induced the production of ISGs that suppress viral replication and budding. Ag_2S nanocrystals (NCs), another type of QD, were also found to positively regulate ISGs and the expression of proinflammatory cytokines.[74] However, among inorganic NPs, the most commonly employed NPs in vaccine design are AuNPs. Sekimukai et al. discovered that AuNPs can act as both an antigen carrier for the SARS-CoV spike *S* protein and an adjuvant.[121] AuNPs bind to the *S* protein via electrostatic interactions, forming a protein corona around the AuNPs. Mice immunized with these NPs showed Th1 and Th2 responses; however, these responses were accompanied by allergic inflammation and eosinophilic infiltration. Chen et al. utilized AuNPs to formulate synthetic VLPs (sVLPs) by incubating 100 nm AuNPs in a solution containing the spike *S* protein of avian coronavirus infectious bronchitis virus (IBV), as shown in Figure 14.[122] Following removal of free protein, antigen-loaded AuNPs were recovered that resembled natural viral proteins, as seen in Figure 14. Protein corona formation increased the NP size to 139 nm, which remained stable over a 7 day period, with each particle retaining approximately 200−250 spike proteins. Compared to inoculation with free proteins, vaccination with these synthetic VLPs showed enhanced lymphatic antigen delivery (6-fold), stronger antibody titers, increased T cell response, and reduced symptoms (see Figure 14). Thus, there are multiple advantages to using AuNPs as next-generation vaccine delivery agents. (1) Inorganic NPs such as AuNPs have high surface energy, leading to spontaneous protein corona formation.[121] As a result, a smaller amount of antigen is required than VLPs to make antigen-exposing NPs of sizes comparable to those of coronaviruses, generating $CD4^+$ T cell and B cell responses.[147] Easy functionalization of AuNPs allows the loading of various other nucleic acids as well. (2) With the NP acting as an adjuvant itself, additional adjuvants are not necessary.[121,147] (3) AuNPs used as antigen carriers also stimulate phagocytic activity of lymphoid cells, stimulate APCs, and induce the release of inflammatory mediators.[147] Localization of AuNPs to

https://dx.doi.org/10.1021/acsanm.0c01978
ACS Appl. Nano Mater. 2020, 3, 8557−8580

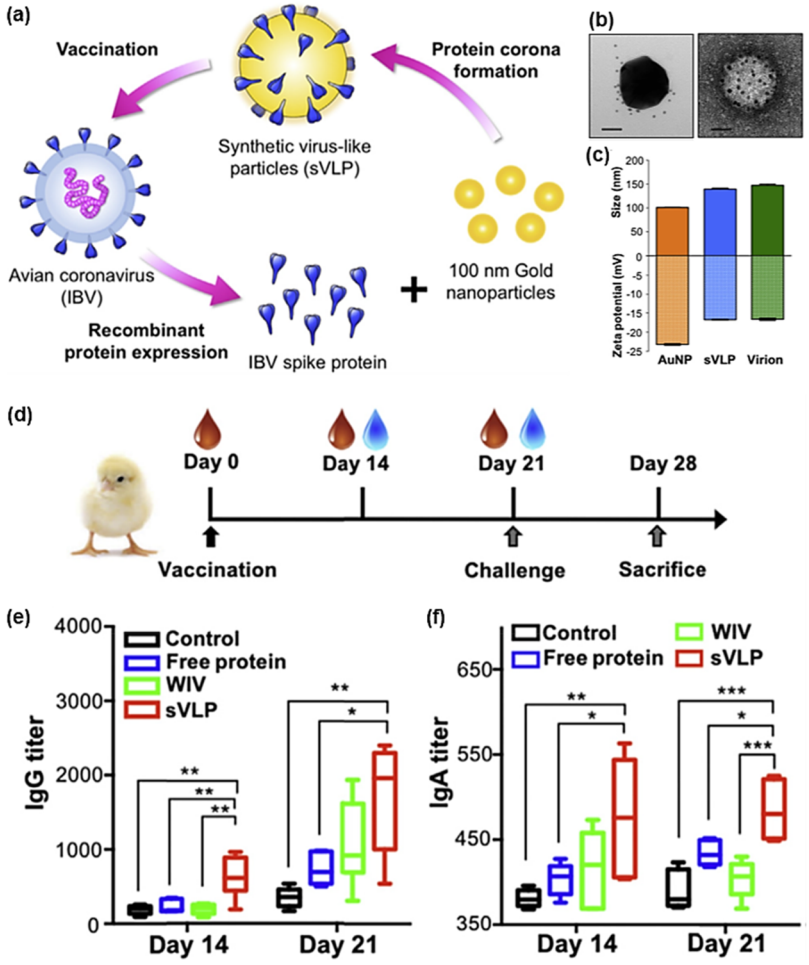

Figure 14. (a) Schematic depiction of the preparation of avian coronavirus sVLPs. sVLPs are prepared in optimized mixtures containing viral proteins and 100 nm gold nanoparticles via spontaneous protein corona formation. (b) Transmission electron microscopy of sVLPs (left) and native IBV virions (right) following immunogold staining against IBV spike proteins. Scale bars = 50 nm. (c) Size and zeta potential of AuNPs, sVLPs, and native IBV virions as analyzed by nanoparticle tracking analysis. Bars represent the mean ± s.d. (n = 3). (d) Vaccination, tissue sample collection, and virus challenge schedule in an avian model of coronavirus infection. (e) Virus-specific serum IgG titers observed in animals vaccinated with free proteins, a commercial whole inactivated virus (WIV) vaccine, and sVLPs. Lines and boxes represent the upper extreme; 25th, 50th, and 75th percentiles; and lower extreme (n = 6). (f) Virus-specific serum IgA titers in animals vaccinated with the different formulations. Lines and boxes represent the upper extreme; 25th, 50th, and 75th percentiles; and lower extreme (n = 6). Reproduced with permission from ref 122. Copyright 2016 Elsevier.

lymphatic tissues and cells is notable, as it mimics what occurs during a natural infection. AuNPs primarily enter cells via phagocytosis, stimulating macrophages, DCs, and lymphocytes.[147] Phagocytosis of NPs is determined by their size and shape.[147] AuNPs with dimensions of 40−100 nm are ideal for phagocytosis, while shape dependence follows the order ellipsoid > spheres > rods > cubes, although in some cases, rods are internalized better than spheres.[118,148,149] However, larger spherical virus-like AuNPs generate the strongest antibody responses. (4) AuNPs have good stability and low cytotoxicity.[88,148]

5. SUMMARY AND PERSPECTIVES

5.1. Nanoparticles for Diagnostics. NPs have been applied to various kinds of virus detection methods. Metal NPs and QDs with unique optical properties have the advantages of enhanced sensitivity for optical biosensing. Meanwhile, MNPs are mainly applied to the virus extraction process due to their magnetic properties. Additionally, the nanohybrid structures combine the advantages of each type of NP to improve the efficiency of virus detection. Recently, NP-based virus detection has been reported as a promising technique to detect the recently discovered SARS-CoV-2, the virus that causes COVID-19. With further research and development, NPs will undoubtedly play an important role in improving not only coronavirus detection efficiency but also other biological pathogen diagnoses.

5.2. Nanoparticles for Therapeutics. Overall, the studies covered in this section show that various NPs can be used to design drugs aimed at disrupting the attachment of SARS-CoV-2 to the ACE2 receptor and blocking the cell entry process while themselves remaining largely nontoxic toward the host cells. Effective antiviral therapies, especially in the early stage of infection, are vitally important to halt viral proliferation long enough for the immune system to respond to the virus and limit cellular damage inflicted by viral invasion as well as to minimize genetic mutations caused by the high replication frequency of the virus, which might lead to therapeutic resistance. NPs with various structures, compositions, and conjugations have been fabricated and evaluated in

https://dx.doi.org/10.1021/acsanm.0c01978
ACS Appl. Nano Mater. 2020, 3, 8557−8580

multiple conditions as highly effective enhancements or alternatives to many existing antiviral therapeutics associated with increasing drug resistance. The antiviral performance, stability, and biocompatibility of these NPs have been rigorously investigated on different human-infecting viruses ranging from members of the coronavirus family to other viruses with close structural similarity to SARS-CoV-2 itself. Using novel antiviral approaches with flexible combinations, many NPs have also been demonstrated to be effective against a broad spectrum of viruses with minimal cytotoxicity, suggesting that these NPs are good research candidates for NP-based antiviral therapies to fight the COVID-19 pandemic.

5.3. Nanoparticles as Immunogenic Agents for Vaccines. Overall, the studies covered in this section offer valuable insight needed for the development of vaccines for COVID-19. The following four conclusions can be drawn: (1) Self-assembled VLPs, template-based and supported VLPs, and synthetic VLPs can all be systematically formulated in sizes and shapes that mimic those of original coronaviruses. These features help induce strong immune responses while avoiding exposure to the virulent genetic components of the virus itself. (2) Repetitive decoration of antigens on the surface of NP vaccines can enhance immune responses, even when using smaller subsets of the proteins; this effect can be further enhanced by matching the natural configuration of the epitopes. Vaccine development has typically exploited coronavirus *S* protein epitopes, but *N* protein epitopes can also be utilized to design broad-spectrum vaccines. (3) NPs offer the opportunity to combine antigen delivery abilities with adjuvant properties. (4) Vaccines targeted specifically toward mucosal cells, DCs, and lymph nodes generate stronger localized immune responses against respiratory viruses such as SARS-CoV-2. Nanosized particles (40−200 nm) are especially suitable for targeted delivery to mucosal and alveolar structures, mimicking natural infection routes and inducing direct immune responses in the worst affected tissues.

Thus, NPs are expected to play a major role in the fight against COVID-19. The optical and magnetic properties of various NPs can be utilized for building diagnostic test kits. The stark morphological and physicochemical similarities of SARS-CoV-2 with synthetic NPs also make NPs a powerful tool for intervention. NPs can be systematically functionalized with various proteins, polymers, and functional groups to perform specific inhibitory functions while also acting as excellent delivery vehicles. NPs offer possibilities for fast and safe vaccine development using subunit proteins instead of whole viruses. Additionally, NPs can also be utilized to make broad-spectrum respiratory drugs and vaccines that can protect us from seasonal viruses and prepare us for future pandemics as well.

AUTHOR INFORMATION

Corresponding Author

T. Randall Lee − *Department of Chemistry and the Texas Center for Superconductivity, University of Houston, Houston, Texas 77204-5003, United States;* orcid.org/0000-0001-9584-8861; Email: trlee@uh.edu

Authors

Riddhiman Medhi − *Department of Chemistry and the Texas Center for Superconductivity, University of Houston, Houston, Texas 77204-5003, United States;* orcid.org/0000-0002-2368-2468

Pannaree Srinoi − *Department of Chemistry and the Texas Center for Superconductivity, University of Houston, Houston, Texas 77204-5003, United States;* orcid.org/0000-0003-4400-468X

Nhat Ngo − *Department of Chemistry and the Texas Center for Superconductivity, University of Houston, Houston, Texas 77204-5003, United States;* orcid.org/0000-0001-5710-1601

Hung-Vu Tran − *Department of Chemistry and the Texas Center for Superconductivity, University of Houston, Houston, Texas 77204-5003, United States;* orcid.org/0000-0001-8536-2737

Complete contact information is available at: https://pubs.acs.org/10.1021/acsanm.0c01978

Notes

The authors declare no competing financial interest.

ACKNOWLEDGMENTS

We thank the Air Force Office of Scientific Research (AFOSR FA9550-18-1-0094), the Robert A. Welch Foundation (E-1320), the Texas Center for Superconductivity, and the University of Houston Advanced Manufacturing Institute for generously supporting this research.

REFERENCES

(1) Chan, J. F. -W.; Yuan, S.; Kok, K.-H.; To, K. K. -W.; Chu, H.; Yang, J.; Xing, F.; Liu, J.; Yip, C. C. -Y.; Poon, R. W. -S.; Tsoi, H.-W.; Lo, S. K. -F.; Chan, K.-H.; Poon, V. K. -M.; Chan, W.-M.; Ip, J. D.; Cai, J.-P.; Cheng, V. C. -C.; Chen, H.; Hui, C. K. -M.; Yuen, K.-Y. A Familial Cluster of Pneumonia Associated with the 2019 Novel Coronavirus Indicating Person-to-Person Transmission: A Study of a Family Cluster. *Lancet* **2020**, *395*, 514−523.

(2) Huang, C.; Wang, Y.; Li, X.; Ren, L.; Zhao, J.; Hu, Y.; Zhang, L.; Fan, G.; Xu, J.; Gu, X.; Cheng, Z.; Yu, T.; Xia, J.; Wei, Y.; Wu, W.; Xie, X.; Yin, W.; Li, H.; Liu, M.; Xiao, Y.; Gao, H.; Guo, L.; Xie, J.; Wang, G.; Jiang, R.; Gao, Z.; Jin, Q.; Wang, J.; Cao, B. Clinical Features of Patients Infected with 2019 Novel Coronavirus in Wuhan, China. *Lancet* **2020**, *395*, 497−506.

(3) Wrapp, D.; Wang, N.; Corbett, K. S.; Goldsmith, J. A.; Hsieh, C.-L.; Abiona, O.; Graham, B. S.; McLellan, J. S. Cryo-EM Structure of the 2019-Ncov Spike in the Prefusion Conformation. *Science* **2020**, *367*, 1260−1263.

(4) Zhang, L.; Lin, D.; Sun, X.; Curth, U.; Drosten, C.; Sauerhering, L.; Becker, S.; Rox, K.; Hilgenfeld, R. Crystal Structure of SARS-CoV-2 Main Protease Provides a Basis for Design of Improved α-Ketoamide Inhibitors. *Science* **2020**, *368*, 409−412.

(5) Gandhi, M.; Yokoe, D. S.; Havlir, D. V. Asymptomatic Transmission, the Achilles' Heel of Current Strategies to Control Covid-19. *N. Engl. J. Med.* **2020**, *382*, 2158−2160.

(6) Rinaldi, A. Free, at Last! The Progress of New Disease Eradication Campaigns for Guinea Worm Disease and Polio, and the Prospect of Tackling Other Diseases. *EMBO Rep.* **2009**, *10*, 215−221.

(7) Sued, O.; Figueroa, M. I.; Cahn, P. Clinical Challenges in HIV/AIDS: Hints for Advancing Prevention and Patient Management Strategies. *Adv. Drug Delivery Rev.* **2016**, *103*, 5−19.

(8) Sharma, J.; Shepardson, K.; Johns, L. L.; Wellham, J.; Avera, J.; Schwarz, B.; Rynda-Apple, A.; Douglas, T. A Self-Adjuvanted, Modular, Antigenic VLP for Rapid Response to Influenza Virus Variability. *ACS Appl. Mater. Interfaces* **2020**, *12*, 18211−18224.

(9) Coleman, C. M.; Liu, Y. V.; Mu, H.; Taylor, J. K.; Massare, M.; Flyer, D. C.; Glenn, G. M.; Smith, G. E.; Frieman, M. B. Purified Coronavirus Spike Protein Nanoparticles Induce Coronavirus Neutralizing Antibodies in Mice. *Vaccine* **2014**, *32*, 3169−3174.

(10) Schindewolf, C.; Menachery, V. D. Middle East Respiratory Syndrome Vaccine Candidates: Cautious Optimism. *Viruses* **2019**, *11*, 74.
(11) Jung, S.-Y.; Kang, K. W.; Lee, E.-Y.; Seo, D.-W.; Kim, H.-L.; Kim, H.; Kwon, T.; Park, H.-L.; Kim, H.; Lee, S.-M.; Nam, J.-H. Heterologous Prime−Boost Vaccination with Adenoviral Vector and Protein Nanoparticles Induces Both Th1 and Th2 Responses against Middle East Respiratory Syndrome Coronavirus. *Vaccine* **2018**, *36*, 3468−3476.
(12) Udugama, B.; Kadhiresan, P.; Kozlowski, H. N.; Malekjahani, A.; Osborne, M.; Li, V. Y. C.; Chen, H.; Mubareka, S.; Gubbay, J. B.; Chan, W. C. W. Diagnosing Covid-19: The Disease and Tools for Detection. *ACS Nano* **2020**, *14*, 3822−3835.
(13) Yan, R.; Zhang, Y.; Li, Y.; Xia, L.; Guo, Y.; Zhou, Q. Structural Basis for the Recognition of SARS-CoV-2 by Full-Length Human ACE2. *Science* **2020**, *367*, 1444−1448.
(14) Chan, W. C. W. Nano Research for Covid-19. *ACS Nano* **2020**, *14*, 3719−3720.
(15) Farka, Z.; Juřík, T.; Kovář, D.; Trnková, L.; Skládal, P. Nanoparticle-Based Immunochemical Biosensors and Assays: Recent Advances and Challenges. *Chem. Rev.* **2017**, *117*, 9973−10042.
(16) Patra, J. K.; Das, G.; Fraceto, L. F.; Campos, E. V. R.; Rodriguez-Torres, M. d. P.; Acosta-Torres, L. S.; Diaz-Torres, L. A.; Grillo, R.; Swamy, M. K.; Sharma, S.; Habtemariam, S.; Shin, H.-S. Nano Based Drug Delivery Systems: Recent Developments and Future Prospects. *J. Nanobiotechnol.* **2018**, *16*, 71.
(17) Han, X.; Xu, K.; Taratula, O.; Farsad, K. Applications of Nanoparticles in Biomedical Imaging. *Nanoscale* **2019**, *11*, 799−819.
(18) Canaparo, R.; Foglietta, F.; Giuntini, F.; Della Pepa, C.; Dosio, F.; Serpe, L. Recent Developments in Antibacterial Therapy: Focus on Stimuli-Responsive Drug-Delivery Systems and Therapeutic Nanoparticles. *Molecules* **2019**, *24*, 1991.
(19) Chen, L.; Liang, J. An Overview of Functional Nanoparticles as Novel Emerging Antiviral Therapeutic Agents. *Mater. Sci. Eng., C* **2020**, *112*, 110924.
(20) Park, J.-E.; Kim, K.; Jung, Y.; Kim, J.-H.; Nam, J.-M. Metal Nanoparticles for Virus Detection. *ChemNanoMat* **2016**, *2*, 927−936.
(21) Corman, V. M.; Landt, O.; Kaiser, M.; Molenkamp, R.; Meijer, A.; Chu, D. K.; Bleicker, T.; Brünink, S.; Schneider, J.; Schmidt, M. L.; Mulders, D. G.; Haagmans, B. L.; van der Veer, B.; van den Brink, S.; Wijsman, L.; Goderski, G.; Romette, J.-L.; Ellis, J.; Zambon, M.; Peiris, M.; Goossens, H.; Reusken, C.; Koopmans, M. P.; Drosten, C. Detection of 2019 Novel Coronavirus (2019-nCoV) by Real-Time RT-PCR. *Euro Surveill.* **2020**, *25*, 2000045.
(22) Shen, M.; Zhou, Y.; Ye, J.; Abdullah Al-Maskri, A. A.; Kang, Y.; Zeng, S.; Cai, S. Recent Advances and Perspectives of Nucleic Acid Detection for Coronavirus. *J. Pharm. Anal.* **2020**, *10*, 97−101.
(23) Emery, S. L.; Erdman, D. D.; Bowen, M. D.; Newton, B. R.; Winchell, J. M.; Meyer, R. F.; Tong, S.; Cook, B. T.; Holloway, B. P.; McCaustland, K. A.; Rota, P. A.; Bankamp, B.; Lowe, L. E.; Ksiazek, T. G.; Bellini, W. J.; Anderson, L. J. Real-Time Reverse Transcription-Polymerase Chain Reaction Assay for SARS-Associated Coronavirus. *Emerging Infect. Dis.* **2004**, *10*, 311−316.
(24) Zhang, Y.; Qu, S.; Xu, L. Progress in the Study of Virus Detection Methods: The Possibility of Alternative Methods to Validate Virus Inactivation. *Biotechnol. Bioeng.* **2019**, *116*, 2095−2102.
(25) Fukushi, S.; Fukuma, A.; Kurosu, T.; Watanabe, S.; Shimojima, M.; Shirato, K.; Iwata-Yoshikawa, N.; Nagata, N.; Ohnishi, K.; Ato, M.; Melaku, S. K.; Sentsui, H.; Saijo, M. Characterization of Novel Monoclonal Antibodies against the MERS-Coronavirus Spike Protein and Their Application in Species-Independent Antibody Detection by Competitive Elisa. *J. Virol. Methods* **2018**, *251*, 22−29.
(26) Mokhtarzadeh, A.; Eivazzadeh-Keihan, R.; Pashazadeh, P.; Hejazi, M.; Gharaatifar, N.; Hasanzadeh, M.; Baradaran, B.; de la Guardia, M. Nanomaterial-Based Biosensors for Detection of Pathogenic Virus. *TrAC, Trends Anal. Chem.* **2017**, *97*, 445−457.
(27) Li, H.; Rothberg, L. Colorimetric Detection of DNA Sequences Based on Electrostatic Interactions with Unmodified Gold Nanoparticles. *Proc. Natl. Acad. Sci. U. S. A.* **2004**, *101*, 14036−14039.
(28) Kim, H.; Park, M.; Hwang, J.; Kim, J. H.; Chung, D.-R.; Lee, K.-s.; Kang, M. Development of Label-Free Colorimetric Assay for MERS-CoV Using Gold Nanoparticles. *ACS Sens.* **2019**, *4*, 1306−1312.
(29) Huang, P.; Wang, H.; Cao, Z.; Jin, H.; Chi, H.; Zhao, J.; Yu, B.; Yan, F.; Hu, X.; Wu, F.; Jiao, C.; Hou, P.; Xu, S.; Zhao, Y.; Feng, N.; Wang, J.; Sun, W.; Wang, T.; Gao, Y.; Yang, S.; Xia, X. A Rapid and Specific Assay for the Detection of MERS-CoV. *Front. Microbiol.* **2018**, *9*, 1101.
(30) Moitra, P.; Alafeef, M.; Dighe, K.; Frieman, M. B.; Pan, D. Selective Naked-Eye Detection of SARS-CoV-2 Mediated by N Gene Targeted Antisense Oligonucleotide Capped Plasmonic Nanoparticles. *ACS Nano* **2020**, *14*, 7617−7627.
(31) Layqah, L. A.; Eissa, S. An Electrochemical Immunosensor for the Corona Virus Associated with the Middle East Respiratory Syndrome Using an Array of Gold Nanoparticle-Modified Carbon Electrodes. *Microchim. Acta* **2019**, *186*, 224.
(32) Lee, Y.; Kang, B.-H.; Kang, M.; Chung, D. R.; Yi, G.-S.; Lee, L. P.; Jeong, K.-H. Nanoplasmonic on-Chip PCR for Rapid Precision Molecular Diagnostics. *ACS Appl. Mater. Interfaces* **2020**, *12*, 12533−12540.
(33) Teengam, P.; Siangproh, W.; Tuantranont, A.; Vilaivan, T.; Chailapakul, O.; Henry, C. S. Multiplex Paper-Based Colorimetric DNA Sensor Using Pyrrolidinyl Peptide Nucleic Acid-Induced AgNPs Aggregation for Detecting MERS-CoV, MTB, and HPV Oligonucleotides. *Anal. Chem.* **2017**, *89*, 5428−5435.
(34) Gong, P.; He, X.; Wang, K.; Tan, W.; Xie, W.; Wu, P.; Li, H. Combination of Functionalized Nanoparticles and Polymerase Chain Reaction-Based Method for SARS-CoV Gene Detection. *J. Nanosci. Nanotechnol.* **2008**, *8*, 293−300.
(35) Zhao, Z.; Cui, H.; Song, W.; Ru, X.; Zhou, W.; Yu, X. A Simple Magnetic Nanoparticles-Based Viral RNA Extraction Method for Efficient Detection of SARS-CoV-2. *BioRxiv* **2020**.
(36) Roh, C.; Jo, S. K. Quantitative and Sensitive Detection of SARS Coronavirus Nucleocapsid Protein Using Quantum Dots-Conjugated RNA Aptamer on Chip. *J. Chem. Technol. Biotechnol.* **2011**, *86*, 1475−1479.
(37) Ahmed, S. R.; Nagy, É.; Neethirajan, S. Self-Assembled Star-Shaped Chiroplasmonic Gold Nanoparticles for an Ultrasensitive Chiro-Immunosensor for Viruses. *RSC Adv.* **2017**, *7*, 40849−40857.
(38) Ahmed, S. R.; Kang, S. W.; Oh, S.; Lee, J.; Neethirajan, S. Chiral Zirconium Quantum Dots: A New Class of Nanocrystals for Optical Detection of Coronavirus. *Heliyon* **2018**, *4*, e00766.
(39) Fong, K. E.; Yung, L. -Y. L. Localized Surface Plasmon Resonance: A Unique Property of Plasmonic Nanoparticles for Nucleic Acid Detection. *Nanoscale* **2013**, *5*, 12043−12071.
(40) Unser, S.; Bruzas, I.; He, J.; Sagle, L. Localized Surface Plasmon Resonance Biosensing: Current Challenges and Approaches. *Sensors* **2015**, *15*, 15684−15716.
(41) Srinoi, P.; Chen, Y.-T.; Vittur, V.; Marquez, M. D.; Lee, T. R. Bimetallic Nanoparticles: Enhanced Magnetic and Optical Properties for Emerging Biological Applications. *Appl. Sci.* **2018**, *8*, 1106.
(42) Draz, M. S.; Shafiee, H. Applications of Gold Nanoparticles in Virus Detection. *Theranostics* **2018**, *8*, 1985−2017.
(43) Dykman, L. A.; Khlebtsov, N. G. Gold Nanoparticles in Biology and Medicine: Recent Advances and Prospects. *Acta Naturae* **2011**, *3*, 34−55.
(44) Khan, M. S.; Vishakante, G. D.; Siddaramaiah, H. Gold Nanoparticles: A Paradigm Shift in Biomedical Applications. *Adv. Colloid Interface Sci.* **2013**, *199*−*200*, 44−58.
(45) Ghosh, S. K.; Pal, T. Interparticle Coupling Effect on the Surface Plasmon Resonance of Gold Nanoparticles: From Theory to Applications. *Chem. Rev.* **2007**, *107*, 4797−4862.
(46) Qiu, G.; Gai, Z.; Tao, Y.; Schmitt, J.; Kullak-Ublick, G. A.; Wang, J. Dual-Functional Plasmonic Photothermal Biosensors for Highly Accurate Severe Acute Respiratory Syndrome Coronavirus 2 Detection. *ACS Nano* **2020**, *14*, 5268−5277.
(47) Ma, C.; Li, C.; Wang, F.; Ma, N.; Li, X.; Li, Z.; Deng, Y.; Wang, Z.; Xi, Z.; Tang, Y.; He, N. Magnetic Nanoparticles-Based Extraction

https://dx.doi.org/10.1021/acsanm.0c01978
ACS Appl. Nano Mater. 2020, 3, 8557−8580

and Verification of Nucleic Acids from Different Sources. *J. Biomed. Nanotechnol.* **2013**, *9*, 703−709.
(48) Borlido, L.; Azevedo, A. M.; Roque, A. C.; Aires-Barros, M. R. Magnetic Separations in Biotechnology. *Biotechnol. Adv.* **2013**, *31*, 1374−1385.
(49) Chen, Y. T.; Kolhatkar, A. G.; Zenasni, O.; Xu, S.; Lee, T. R. Biosensing Using Magnetic Particle Detection Techniques. *Sensors* **2017**, *17*, 2300.
(50) Rocha-Santos, T. A. P. Sensors and Biosensors Based on Magnetic Nanoparticles. *TrAC, Trends Anal. Chem.* **2014**, *62*, 28−36.
(51) Lee, A. H. F.; Gessert, S. F.; Chen, Y.; Sergeev, N. V.; Haghiri, B. Preparation of Iron Oxide Silica Particles for Zika Viral RNA Extraction. *Heliyon* **2018**, *4*, e00572.
(52) Wang, J.; Ali, Z.; Si, J.; Wang, N.; He, N.; Li, Z. Simultaneous Extraction of DNA and RNA from Hepatocellular Carcinoma (Hep G2) Based on Silica-Coated Magnetic Nanoparticles. *J. Nanosci. Nanotechnol.* **2017**, *17*, 802−806.
(53) Zhang, H.; Xu, T.; Li, C.-W.; Yang, M. A Microfluidic Device with Microbead Array for Sensitive Virus Detection and Genotyping Using Quantum Dots as Fluorescence Labels. *Biosens. Bioelectron.* **2010**, *25*, 2402−2407.
(54) Wang, T.; Zheng, Z.; Zhang, X.-E.; Wang, H. Quantum Dot-Fluorescence In Situ Hybridisation for Ectromelia Virus Detection Based on Biotin−Streptavidin Interactions. *Talanta* **2016**, *158*, 179−184.
(55) Papp, I.; Sieben, C.; Ludwig, K.; Roskamp, M.; Böttcher, C.; Schlecht, S.; Herrmann, A.; Haag, R. Inhibition of Influenza Virus Infection by Multivalent Sialic-Acid-Functionalized Gold Nanoparticles. *Small* **2010**, *6*, 2900−2906.
(56) Sametband, M.; Shukla, S.; Meningher, T.; Hirsh, S.; Mendelson, E.; Sarid, R.; Gedanken, A.; Mandelboim, M. Effective Multi-Strain Inhibition of Influenza Virus by Anionic Gold Nanoparticles. *MedChemComm* **2011**, *2*, 421−423.
(57) Cagno, V.; Andreozzi, P.; D'Alicarnasso, M.; Jacob Silva, P.; Mueller, M.; Galloux, M.; Le Goffic, R.; Jones, S. T.; Vallino, M.; Hodek, J.; Weber, J.; Sen, S.; Janeček, E.-R.; Bekdemir, A.; Sanavio, B.; Martinelli, C.; Donalisio, M.; Rameix Welti, M.-A.; Eleouet, J.-F.; Han, Y.; Kaiser, L.; Vukovic, L.; Tapparel, C.; Král, P.; Krol, S.; Lembo, D.; Stellacci, F. Broad-Spectrum Non-Toxic Antiviral Nanoparticles with a Virucidal Inhibition Mechanism. *Nat. Mater.* **2018**, *17*, 195−203.
(58) Kim, J.; Yeom, M.; Lee, T.; Kim, H.-O.; Na, W.; Kang, A.; Lim, J.-W.; Park, G.; Park, C.; Song, D.; Haam, S. Porous Gold Nanoparticles for Attenuating Infectivity of Influenza a Virus. *J. Nanobiotechnol.* **2020**, *18*, 54.
(59) Huang, X.; Li, M.; Xu, Y.; Zhang, J.; Meng, X.; An, X.; Sun, L.; Guo, L.; Shan, X.; Ge, J.; Chen, J.; Luo, Y.; Wu, H.; Zhang, Y.; Jiang, Q.; Ning, X. Novel Gold Nanorod-Based HR1 Peptide Inhibitor for Middle East Respiratory Syndrome Coronavirus. *ACS Appl. Mater. Interfaces* **2019**, *11*, 19799−19807.
(60) Yang, X. X.; Li, C. M.; Huang, C. Z. Curcumin Modified Silver Nanoparticles for Highly Efficient Inhibition of Respiratory Syncytial Virus Infection. *Nanoscale* **2016**, *8*, 3040−3048.
(61) Chen, Y.-N.; Hsueh, Y.-H.; Hsieh, C.- T.; Tzou, D.-Y.; Chang, P.-L. Antiviral Activity of Graphene−Silver Nanocomposites against Non-Enveloped and Enveloped Viruses. *Int. J. Environ. Res. Public Health* **2016**, *13*, 430.
(62) Lv, X.; Wang, P.; Bai, R.; Cong, Y.; Suo, S.; Ren, X.; Chen, C. Inhibitory Effect of Silver Nanomaterials on Transmissible Virus-Induced Host Cell Infections. *Biomaterials* **2014**, *35*, 4195−4203.
(63) Li, Y.; Lin, Z.; Zhao, M.; Xu, T.; Wang, C.; Hua, L.; Wang, H.; Xia, H.; Zhu, B. Silver Nanoparticle Based Codelivery of Oseltamivir to Inhibit the Activity of the H1N1 Influenza Virus through ROS-Mediated Signaling Pathways. *ACS Appl. Mater. Interfaces* **2016**, *8*, 24385−24393.
(64) Lin, Z.; Li, Y.; Guo, M.; Xu, T.; Wang, C.; Zhao, M.; Wang, H.; Chen, T.; Zhu, B. The Inhibition of H1N1 Influenza Virus-Induced Apoptosis by Silver Nanoparticles Functionalized with Zanamivir. *RSC Adv.* **2017**, *7*, 742−750.
(65) Morris, D.; Ansar, M.; Speshock, J.; Ivanciuc, T.; Qu, Y.; Casola, A.; Garofalo, R. Antiviral and Immunomodulatory Activity of Silver Nanoparticles in Experimental RSV Infection. *Viruses* **2019**, *11*, 732.
(66) Osminkina, L. A.; Timoshenko, V. Y.; Shilovsky, I. P.; Kornilaeva, G. V.; Shevchenko, S. N.; Gongalsky, M. B.; Tamarov, K. P.; Abramchuk, S. S.; Nikiforov, V. N.; Khaitov, M. R.; Karamov, E. V. Porous Silicon Nanoparticles as Scavengers of Hazardous Viruses. *J. Nanopart. Res.* **2014**, *16*, 2430.
(67) Lin, Z.; Li, Y.; Guo, M.; Xiao, M.; Wang, C.; Zhao, M.; Xu, T.; Xia, Y.; Zhu, B. Inhibition of H1N1 Influenza Virus by Selenium Nanoparticles Loaded with Zanamivir through P38 and Jnk Signaling Pathways. *RSC Adv.* **2017**, *7*, 35290−35296.
(68) Li, Y.; Lin, Z.; Guo, M.; Zhao, M.; Xia, Y.; Wang, C.; Xu, T.; Zhu, B. Inhibition of H1N1 Influenza Virus-Induced Apoptosis by Functionalized Selenium Nanoparticles with Amantadine through ROS-Mediated AKT Signaling Pathways. *Int. J. Nanomed.* **2018**, *13*, 2005−2016.
(69) Lin, Z.; Li, Y.; Gong, G.; Xia, Y.; Wang, C.; Chen, Y.; Hua, L.; Zhong, J.; Tang, Y.; Liu, X.; Zhu, B. Restriction of H1N1 Influenza Virus Infection by Selenium Nanoparticles Loaded with Ribavirin Via Resisting Caspase-3 Apoptotic Pathway. *Int. J. Nanomed.* **2018**, *13*, 5787−5797.
(70) Li, Y.; Lin, Z.; Guo, M.; Xia, Y.; Zhao, M.; Wang, C.; Xu, T.; Chen, T.; Zhu, B. Inhibitory Activity of Selenium Nanoparticles Functionalized with Oseltamivir on H1N1 Influenza Virus. *Int. J. Nanomed.* **2017**, *12*, 5733−5743.
(71) Ghaffari, H.; Tavakoli, A.; Moradi, A.; Tabarraei, A.; Bokharaei-Salim, F.; Zahmatkeshan, M.; Farahmand, M.; Javanmard, D.; Kiani, S. J.; Esghaei, M.; Pirhajati-Mahabadi, V.; Monavari, S. H.; Ataei-Pirkooh, A. Inhibition of H1N1 Influenza Virus Infection by Zinc Oxide Nanoparticles: Another Emerging Application of Nanomedicine. *J. Biomed. Sci.* **2019**, *26*, 70.
(72) De Souza e Silva, J. M.; Hanchuk, T. D. M.; Santos, M. I.; Kobarg, J.; Bajgelman, M. C.; Cardoso, M. B. Viral Inhibition Mechanism Mediated by Surface-Modified Silica Nanoparticles. *ACS Appl. Mater. Interfaces* **2016**, *8*, 16564−16572.
(73) Bromberg, L.; Bromberg, D. J.; Hatton, T. A.; Bandín, I.; Concheiro, A.; Alvarez-Lorenzo, C. Antiviral Properties of Polymeric Aziridine- and Biguanide-Modified Core−Shell Magnetic Nanoparticles. *Langmuir* **2012**, *28*, 4548−4558.
(74) Du, T.; Liang, J.; Dong, N.; Lu, J.; Fu, Y.; Fang, L.; Xiao, S.; Han, H. Glutathione-Capped Ag_2S Nanoclusters Inhibit Coronavirus Proliferation through Blockage of Viral RNA Synthesis and Budding. *ACS Appl. Mater. Interfaces* **2018**, *10*, 4369−4378.
(75) Łoczechin, A.; Séron, K.; Barras, A.; Giovanelli, E.; Belouzard, S.; Chen, Y.-T.; Metzler-Nolte, N.; Boukherroub, R.; Dubuisson, J.; Szunerits, S. Functional Carbon Quantum Dots as Medical Countermeasures to Human Coronavirus. *ACS Appl. Mater. Interfaces* **2019**, *11*, 42964−42974.
(76) Ting, D.; Dong, N.; Fang, L.; Lu, J.; Bi, J.; Xiao, S.; Han, H. Multisite Inhibitors for Enteric Coronavirus: Antiviral Cationic Carbon Dots Based on Curcumin. *ACS Appl. Nano Mater.* **2018**, *1*, 5451−5459.
(77) Tong, T.; Hu, H.; Zhou, J.; Deng, S.; Zhang, X.; Tang, W.; Fang, L.; Xiao, S.; Liang, J. Glycyrrhizic-Acid-Based Carbon Dots with High Antiviral Activity by Multisite Inhibition Mechanisms. *Small* **2020**, *16*, 1906206.
(78) Huang, S.; Gu, J.; Ye, J.; Fang, B.; Wan, S.; Wang, C.; Ashraf, U.; Li, Q.; Wang, X.; Shao, L.; Song, Y.; Zheng, X.; Cao, F.; Cao, S. Benzoxazine Monomer Derived Carbon Dots as a Broad-Spectrum Agent to Block Viral Infectivity. *J. Colloid Interface Sci.* **2019**, *542*, 198−206.
(79) Zoppe, J. O.; Ruottinen, V.; Ruotsalainen, J.; Rönkkö, S.; Johansson, L.-S.; Hinkkanen, A.; Järvinen, K.; Seppälä, J. Synthesis of Cellulose Nanocrystals Carrying Tyrosine Sulfate Mimetic Ligands and Inhibition of Alphavirus Infection. *Biomacromolecules* **2014**, *15*, 1534−1542.

https://dx.doi.org/10.1021/acsanm.0c01978
ACS Appl. Nano Mater. 2020, 3, 8557−8580

(80) Lima, T. L. C.; Feitosa, R. D. C.; Dos Santos-Silva, E.; Dos Santos-Silva, A. M.; Siqueira, E. M. D. S.; Machado, P. R. L.; Cornélio, A. M.; Do Egito, E. S. T.; Fernandes-Pedrosa, M. D. F.; Farias, K. J. S.; Da Silva-Júnior, A. A. Improving Encapsulation of Hydrophilic Chloroquine Diphosphate into Biodegradable Nanoparticles: A Promising Approach against Herpes Virus Simplex-1 Infection. *Pharmaceutics* **2018**, *10*, 255.
(81) Kong, B.; Moon, S.; Kim, Y.; Heo, P.; Jung, Y.; Yu, S.-H.; Chung, J.; Ban, C.; Kim, Y. H.; Kim, P.; Hwang, B. J.; Chung, W.-J.; Shin, Y.-K.; Seong, B. L.; Kweon, D.-H. Virucidal Nano-Perforator of Viral Membrane Trapping Viral Rnas in the Endosome. *Nat. Commun.* **2019**, *10*, 185.
(82) Hoffmann, M.; Kleine-Weber, H.; Schroeder, S.; Krüger, N.; Herrler, T.; Erichsen, S.; Schiergens, T. S.; Herrler, G.; Wu, N.-H.; Nitsche, A.; Müller, M. A.; Drosten, C.; Pöhlmann, S. SARS-CoV-2 Cell Entry Depends on ACE2 and TMPRSS2 and Is Blocked by a Clinically Proven Protease Inhibitor. *Cell* **2020**, *181*, 271−280.
(83) Ou, X.; Liu, Y.; Lei, X.; Li, P.; Mi, D.; Ren, L.; Guo, L.; Guo, R.; Chen, T.; Hu, J.; Xiang, Z.; Mu, Z.; Chen, X.; Chen, J.; Hu, K.; Jin, Q.; Wang, J.; Qian, Z. Characterization of Spike Glycoprotein of SARS-CoV-2 on Virus Entry and Its Immune Cross-Reactivity with SARS-CoV. *Nat. Commun.* **2020**, *11*, 1620.
(84) Wang, Q.; Zhang, Y.; Wu, L.; Niu, S.; Song, C.; Zhang, Z.; Lu, G.; Qiao, C.; Hu, Y.; Yuen, K.-Y.; Wang, Q.; Zhou, H.; Yan, J.; Qi, J. Structural and Functional Basis of SARS-CoV-2 Entry by Using Human ACE2. *Cell* **2020**, *181*, 894−904.
(85) Hu, T. Y.; Frieman, M.; Wolfram, J. Insights from Nanomedicine into Chloroquine Efficacy against Covid-19. *Nat. Nanotechnol.* **2020**, *15*, 247−249.
(86) Iannazzo, D.; Pistone, A.; Ferro, S.; De Luca, L.; Monforte, A. M.; Romeo, R.; Buemi, M. R.; Pannecouque, C. Graphene Quantum Dots Based Systems as HIV Inhibitors. *Bioconjugate Chem.* **2018**, *29*, 3084−3093.
(87) Galdiero, S.; Falanga, A.; Vitiello, M.; Cantisani, M.; Marra, V.; Galdiero, M. Silver Nanoparticles as Potential Antiviral Agents. *Molecules* **2011**, *16*, 8894−8918.
(88) Yen, H.-J.; Hsu, S.-H.; Tsai, C.-L. Cytotoxicity and Immunological Response of Gold and Silver Nanoparticles of Different Sizes. *Small* **2009**, *5*, 1553−1561.
(89) Johnston, H. J.; Hutchison, G.; Christensen, F. M.; Peters, S.; Hankin, S.; Stone, V. A Review of the In Vivo and In Vitro Toxicity of Silver and Gold Particulates: Particle Attributes and Biological Mechanisms Responsible for the Observed Toxicity. *Crit. Rev. Toxicol.* **2010**, *40*, 328−346.
(90) Bar-Ilan, O.; Albrecht, R. M.; Fako, V. E.; Furgeson, D. Y. Toxicity Assessments of Multisized Gold and Silver Nanoparticles in Zebrafish Embryos. *Small* **2009**, *5*, 1897−1910.
(91) Li, Y.; Lin, Z.; Gong, G.; Guo, M.; Xu, T.; Wang, C.; Zhao, M.; Xia, Y.; Tang, Y.; Zhong, J.; Chen, Y.; Hua, L.; Huang, Y.; Zeng, F.; Zhu, B. Inhibition of H1N1 Influenza Virus-Induced Apoptosis by Selenium Nanoparticles Functionalized with Arbidol through ROS-Mediated Signaling Pathways. *J. Mater. Chem. B* **2019**, *7*, 4252−4262.
(92) Milewska, A.; Kaminski, K.; Ciejka, J.; Kosowicz, K.; Zeglen, S.; Wojarski, J.; Nowakowska, M.; Szczubiałka, K.; Pyrc, K. HTCC: Broad Range Inhibitor of Coronavirus Entry. *PLoS One* **2016**, *11*, e0156552.
(93) Raghuwanshi, D.; Mishra, V.; Das, D.; Kaur, K.; Suresh, M. R. Dendritic Cell Targeted Chitosan Nanoparticles for Nasal DNA Immunization against SARS CoV Nucleocapsid Protein. *Mol. Pharmaceutics* **2012**, *9*, 946−956.
(94) Alghrair, Z. K.; Fernig, D. G.; Ebrahimi, B. Enhanced Inhibition of Influenza Virus Infection by Peptide-Noble-Metal Nanoparticle Conjugates. *Beilstein J. Nanotechnol.* **2019**, *10*, 1038−1047.
(95) Mori, Y.; Ono, T.; Miyahira, Y.; Nguyen, V. Q.; Matsui, T.; Ishihara, M. Antiviral Activity of Silver Nanoparticle/Chitosan Composites against H1n1 Influenza a Virus. *Nanoscale Res. Lett.* **2013**, *8*, 93−93.
(96) Du, T.; Lu, J.; Liu, L.; Dong, N.; Fang, L.; Xiao, S.; Han, H. Antiviral Activity of Graphene Oxide−Silver Nanocomposites by Preventing Viral Entry and Activation of the Antiviral Innate Immune Response. *ACS Appl. Bio Mater.* **2018**, *1*, 1286−1293.
(97) Du, T.; Liang, J.; Dong, N.; Liu, L.; Fang, L.; Xiao, S.; Han, H. Carbon Dots as Inhibitors of Virus by Activation of Type I Interferon Response. *Carbon* **2016**, *110*, 278−285.
(98) Sharma, V.; Kaushik, S.; Pandit, P.; Dhull, D.; Yadav, J. P.; Kaushik, S. Green Synthesis of Silver Nanoparticles from Medicinal Plants and Evaluation of Their Antiviral Potential against Chikungunya Virus. *Appl. Microbiol. Biotechnol.* **2019**, *103*, 881−891.
(99) Yang, X. X.; Li, C. M.; Huang, C. Z. Curcumin Modified Silver Nanoparticles for Highly Efficient Inhibition of Respiratory Syncytial Virus Infection. *Nanoscale* **2016**, *8*, 3040−3048.
(100) Elechiguerra, J. L.; Burt, J. L.; Morones, J. R.; Camacho-Bragado, A.; Gao, X.; Lara, H. H.; Yacaman, M. J. Interaction of Silver Nanoparticles with HIV-1. *J. Nanobiotechnol.* **2005**, *3*, 6.
(101) Bowman, M.-C.; Ballard, T. E.; Ackerson, C. J.; Feldheim, D. L.; Margolis, D. M.; Melander, C. Inhibition of HIV Fusion with Multivalent Gold Nanoparticles. *J. Am. Chem. Soc.* **2008**, *130*, 6896−6897.
(102) Di Gianvincenzo, P.; Marradi, M.; Martínez-Ávila, O. M.; Bedoya, L. M.; Alcamí, J.; Penadés, S. Gold Nanoparticles Capped with Sulfate-Ended Ligands as Anti-HIV Agents. *Bioorg. Med. Chem. Lett.* **2010**, *20*, 2718−2721.
(103) Rosemary Bastian, A.; Nangarlia, A.; Bailey, L. D.; Holmes, A.; Kalyana Sundaram, R. V.; Ang, C.; Moreira, D. R.; Freedman, K.; Duffy, C.; Contarino, M.; Abrams, C.; Root, M.; Chaiken, I. Mechanism of Multivalent Nanoparticle Encounter with HIV-1 for Potency Enhancement of Peptide Triazole Virus Inactivation. *J. Biol. Chem.* **2015**, *290*, 529−543.
(104) Speshock, J. L.; Murdock, R. C.; Braydich-Stolle, L. K.; Schrand, A. M.; Hussain, S. M. Interaction of Silver Nanoparticles with Tacaribe Virus. *J. Nanobiotechnol.* **2010**, *8*, 19.
(105) Baram-Pinto, D.; Shukla, S.; Perkas, N.; Gedanken, A.; Sarid, R. Inhibition of Herpes Simplex Virus Type 1 Infection by Silver Nanoparticles Capped with Mercaptoethane Sulfonate. *Bioconjugate Chem.* **2009**, *20*, 1497−1502.
(106) Orłowski, P.; Kowalczyk, A.; Tomaszewska, E.; Ranoszek-Soliwoda, K.; Węgrzyn, A.; Grzesiak, J.; Celichowski, G.; Grobelny, J.; Eriksson, K.; Krzyzowska, M. Antiviral Activity of Tannic Acid Modified Silver Nanoparticles: Potential to Activate Immune Response in Herpes Genitalis. *Viruses* **2018**, *10*, 524.
(107) Gaikwad, S.; Ingle, A.; Gade, A.; Rai, M.; Falanga, A.; Incoronato, N.; Russo, L.; Galdiero, S.; Galdiero, M. Antiviral Activity of Mycosynthesized Silver Nanoparticles against Herpes Simplex Virus and Human Parainfluenza Virus Type 3. *Int. J. Nanomed.* **2013**, *8*, 4303−4314.
(108) Qin, T.; Ma, R.; Yin, Y.; Miao, X.; Chen, S.; Fan, K.; Xi, J.; Liu, Q.; Gu, Y.; Yin, Y.; Hu, J.; Liu, X.; Peng, D.; Gao, L. Catalytic Inactivation of Influenza Virus by Iron Oxide Nanozyme. *Theranostics* **2019**, *9*, 6920−6935.
(109) Lim, M. E.; Lee, Y. L.; Zhang, Y.; Chu, J. J. Photodynamic Inactivation of Viruses Using Upconversion Nanoparticles. *Biomaterials* **2012**, *33*, 1912−1920.
(110) Meléndez-Villanueva, M. A.; Morán-Santibañez, K.; Martínez-Sanmiguel, J. J.; Rangel-López, R.; Garza-Navarro, M. A.; Rodríguez-Padilla, C.; Zarate-Triviño, D. G.; Trejo-Ávila, L. M. Virucidal Activity of Gold Nanoparticles Synthesized by Green Chemistry Using Garlic Extract. *Viruses* **2019**, *11*, 1111.
(111) Wang, Z.; Liu, H.; Yang, S. H.; Wang, T.; Liu, C.; Cao, Y. C. Nanoparticle-Based Artificial RNA Silencing Machinery for Antiviral Therapy. *Proc. Natl. Acad. Sci. U. S. A.* **2012**, *109*, 12387−12392.
(112) Park, S.; Ko, Y. S.; Lee, S. J.; Lee, C.; Woo, K.; Ko, G. Inactivation of Influenza a Virus Via Exposure to Silver Nanoparticle-Decorated Silica Hybrid Composites. *Environ. Sci. Pollut. Res.* **2018**, *25*, 27021−27030.
(113) Botequim, D.; Maia, J.; Lino, M. M. F.; Lopes, L. M. F.; Simões, P. N.; Ilharco, L. M.; Ferreira, L. Nanoparticles and Surfaces Presenting Antifungal, Antibacterial and Antiviral Properties. *Langmuir* **2012**, *28*, 7646−7656.

https://dx.doi.org/10.1021/acsanm.0c01978
ACS Appl. Nano Mater. 2020, 3, 8557−8580

(114) Lara, H. H.; Ayala-Nuñez, N. V.; Ixtepan-Turrent, L.; Rodriguez-Padilla, C. Mode of Antiviral Action of Silver Nanoparticles against HIV-1. *J. Nanobiotechnol.* **2010**, *8*, 1.
(115) Wei, X.; Zhang, G.; Ran, D.; Krishnan, N.; Fang, R. H.; Gao, W.; Spector, S. A.; Zhang, L. T-Cell-Mimicking Nanoparticles Can Neutralize HIV Infectivity. *Adv. Mater.* **2018**, *30*, 1802233.
(116) Bai, Y.; Zhou, Y.; Liu, H.; Fang, L.; Liang, J.; Xiao, S. Glutathione-Stabilized Fluorescent Gold Nanoclusters Vary in Their Influences on the Proliferation of Pseudorabies Virus and Porcine Reproductive and Respiratory Syndrome Virus. *ACS Appl. Nano Mater.* **2018**, *1*, 969−976.
(117) Zhang, J.-M.; An, J. Cytokines, Inflammation, and Pain. *Int. Anesthesiol. Clin.* **2007**, *45*, 27−37.
(118) Lung, P.; Yang, J.; Li, Q. Nanoparticle Formulated Vaccines: Opportunities and Challenges. *Nanoscale* **2020**, *12*, 5746−5763.
(119) Ramshaw, I. A.; Ramsay, A. J.; Karupiah, G.; Rolph, M. S.; Mahalingam, S.; Ruby, J. C. Cytokines and Immunity to Viral Infections. *Immunol. Rev.* **1997**, *159*, 119−135.
(120) Ruby, J.; Bluethmann, H.; Peschon, J. J. Antiviral Activity of Tumor Necrosis Factor (TNF) Is Mediated Via P55 and P75 TNF Receptors. *J. Exp. Med.* **1997**, *186*, 1591−1596.
(121) Sekimukai, H.; Iwata-Yoshikawa, N.; Fukushi, S.; Tani, H.; Kataoka, M.; Suzuki, T.; Hasegawa, H.; Niikura, K.; Arai, K.; Nagata, N. Gold Nanoparticle-Adjuvanted S Protein Induces a Strong Antigen-Specific IgG Response against Severe Acute Respiratory Syndrome-Related Coronavirus Infection, but Fails to Induce Protective Antibodies and Limit Eosinophilic Infiltration in Lungs. *Microbiol. Immunol.* **2020**, *64*, 33−51.
(122) Chen, H.-W.; Huang, C.-Y.; Lin, S.-Y.; Fang, Z.-S.; Hsu, C.-H.; Lin, J.-C.; Chen, Y.-I.; Yao, B.-Y.; Hu, C. -M. J. Synthetic Virus-Like Particles Prepared Via Protein Corona Formation Enable Effective Vaccination in an Avian Model of Coronavirus Infection. *Biomaterials* **2016**, *106*, 111−118.
(123) Coleman, C. M.; Venkataraman, T.; Liu, Y. V.; Glenn, G. M.; Smith, G. E.; Flyer, D. C.; Frieman, M. B. MERS-CoV Spike Nanoparticles Protect Mice from MERS-CoV Infection. *Vaccine* **2017**, *35*, 1586−1589.
(124) Pimentel, T. A. P. F.; Yan, Z.; Jeffers, S. A.; Holmes, K. V.; Hodges, R. S.; Burkhard, P. Peptide Nanoparticles as Novel Immunogens: Design and Analysis of a Prototypic Severe Acute Respiratory Syndrome Vaccine. *Chem. Biol. Drug Des.* **2009**, *73*, 53−61.
(125) Wang, C.; Zheng, X.; Gai, W.; Wong, G.; Wang, H.; Jin, H.; Feng, N.; Zhao, Y.; Zhang, W.; Li, N.; Zhao, G.; Li, J.; Yan, J.; Gao, Y.; Hu, G.; Yang, S.; Xia, X. Novel Chimeric Virus-Like Particles Vaccine Displaying MERS-CoV Receptor-Binding Domain Induce Specific Humoral and Cellular Immune Response in Mice. *Antiviral Res.* **2017**, *140*, 55−61.
(126) Wiley, J. A.; Richert, L. E.; Swain, S. D.; Harmsen, A.; Barnard, D. L.; Randall, T. D.; Jutila, M.; Douglas, T.; Broomell, C.; Young, M.; Harmsen, A. Inducible Bronchus-Associated Lymphoid Tissue Elicited by a Protein Cage Nanoparticle Enhances Protection in Mice against Diverse Respiratory Viruses. *PLoS One* **2009**, *4*, e7142.
(127) Lin, L. C. -W.; Huang, C.-Y.; Yao, B.-Y.; Lin, J.-C.; Agrawal, A.; Algaissi, A.; Peng, B.-H.; Liu, Y.-H.; Huang, P.-H.; Juang, R.-H.; Chang, Y.-C.; Tseng, C.-T.; Chen, H.-W.; Hu, C. -M. J. Viromimetic Sting Agonist-Loaded Hollow Polymeric Nanoparticles for Safe and Effective Vaccination against Middle East Respiratory Syndrome Coronavirus. *Adv. Funct. Mater.* **2019**, *29*, 1807616.
(128) Plummer, E. M.; Manchester, M. Viral Nanoparticles and Virus-Like Particles: Platforms for Contemporary Vaccine Design. *Wiley Interdiscip. Rev. Nanomed. Nanobiotechnol.* **2011**, *3*, 174−196.
(129) Peek, L. J.; Middaugh, C. R.; Berkland, C. Nanotechnology in Vaccine Delivery. *Adv. Drug Delivery Rev.* **2008**, *60*, 915−928.
(130) World Health Organization (WHO). *Draft Landscape of COVID-19 Candidate Vaccines, 2020*. https://www.who.int/publications/m/item/draft-landscape-of-covid-19-candidate-vaccines (accessed Jul 10, 2020).
(131) Kim, Y.-S.; Son, A.; Kim, J.; Kwon, S. B.; Kim, M. H.; Kim, P.; Kim, J.; Byun, Y. H.; Sung, J.; Lee, J.; Yu, J. E.; Park, C.; Kim, Y.-S.; Cho, N.-H.; Chang, J.; Seong, B. L. Chaperna-Mediated Assembly of Ferritin-Based Middle East Respiratory Syndrome-Coronavirus Nanoparticles. *Front. Immunol.* **2018**, *9*, 1093.
(132) Carter, D. C.; Wright, B.; Jerome, W. G.; Rose, J. P.; Wilson, E. A Unique Protein Self-Assembling Nanoparticle with Significant Advantages in Vaccine Development and Production. *J. Nanomater.* **2020**, *2020*, 4297937.
(133) Gelperina, S.; Kisich, K.; Iseman, M. D.; Heifets, L. The Potential Advantages of Nanoparticle Drug Delivery Systems in Chemotherapy of Tuberculosis. *Am. J. Respir. Crit. Care Med.* **2005**, *172*, 1487−1490.
(134) Singh, R.; Lillard, J. W. Nanoparticle-Based Targeted Drug Delivery. *Exp. Mol. Pathol.* **2009**, *86*, 215−223.
(135) Sung, J. C.; Pulliam, B. L.; Edwards, D. A. Nanoparticles for Drug Delivery to the Lungs. *Trends Biotechnol.* **2007**, *25*, 563−570.
(136) Arruebo, M.; Fernández-Pacheco, R.; Ibarra, M. R.; Santamaría, J. Magnetic Nanoparticles for Drug Delivery. *Nano Today* **2007**, *2*, 22−32.
(137) Bryan, W. W.; Medhi, R.; Marquez, M. D.; Rittikulsittichai, S.; Tran, M.; Lee, T. R. Porous Silver-Coated pNIPAM-Co-AAc Hydrogel Nanocapsules. *Beilstein J. Nanotechnol.* **2019**, *10*, 1973−1982.
(138) Tacken, P. J.; de Vries, I. J. M.; Torensma, R.; Figdor, C. G. Dendritic-Cell Immunotherapy: From Ex Vivo Loading to In Vivo Targeting. *Nat. Rev. Immunol.* **2007**, *7*, 790−802.
(139) Ciejka, J.; Wolski, K.; Nowakowska, M.; Pyrc, K.; Szczubiałka, K. Biopolymeric Nano/Microspheres for Selective and Reversible Adsorption of Coronaviruses. *Mater. Sci. Eng., C* **2017**, *76*, 735−742.
(140) Xu, Y.; Yuen, P.-W.; Lam, J. K. -W. Intranasal DNA Vaccine for Protection against Respiratory Infectious Diseases: The Delivery Perspectives. *Pharmaceutics* **2014**, *6*, 378−415.
(141) Tse, G. M. -K.; To, K.-F.; Chan, P. K.-S.; Lo, A. W. I.; Ng, K.-C.; Wu, A.; Lee, N.; Wong, H.-C.; Mak, S.-M.; Chan, K.-F.; Hui, D. S. C.; Sung, J. J. -Y.; Ng, H.-K. Pulmonary Pathological Features in Coronavirus Associated Severe Acute Respiratory Syndrome (SARS). *J. Clin. Pathol.* **2004**, *57*, 260−265.
(142) Gu, J.; Korteweg, C. Pathology and Pathogenesis of Severe Acute Respiratory Syndrome. *Am. J. Pathol.* **2007**, *170*, 1136−1147.
(143) Nascimento, T. L.; Hillaireau, H.; Fattal, E. Nanoscale Particles for Lung Delivery of siRNA. *J. Drug Delivery Sci. Technol.* **2012**, *22*, 99−108.
(144) Wang, F.; Kream, R. M.; Stefano, G. B. An Evidence Based Perspective on mRNA-SARS-CoV-2 Vaccine Development. *Med. Sci. Monit.* **2020**, *26*, 924700.
(145) Liu, C.; Zhou, Q.; Li, Y.; Garner, L. V.; Watkins, S. P.; Carter, L. J.; Smoot, J.; Gregg, A. C.; Daniels, A. D.; Jervey, S.; Albaiu, D. Research and Development on Therapeutic Agents and Vaccines for Covid-19 and Related Human Coronavirus Diseases. *ACS Cent. Sci.* **2020**, *6*, 315−331.
(146) Frede, A.; Neuhaus, B.; Knuschke, T.; Wadwa, M.; Kollenda, S.; Klopfleisch, R.; Hansen, W.; Buer, J.; Bruder, D.; Epple, M.; Westendorf, A. M. Local Delivery of siRNA-Loaded Calcium Phosphate Nanoparticles Abates Pulmonary Inflammation. *Nanomedicine* **2017**, *13*, 2395−2403.
(147) Dykman, L. A.; Khlebtsov, N. G. Immunological Properties of Gold Nanoparticles. *Chem. Sci.* **2017**, *8*, 1719−1735.
(148) Comber, J. D.; Bamezai, A. Gold Nanoparticles (AuNPs): A New Frontier in Vaccine Delivery. *J. Nanomed. Biother. Discovery* **2015**, *5*, e139.
(149) Niikura, K.; Matsunaga, T.; Suzuki, T.; Kobayashi, S.; Yamaguchi, H.; Orba, Y.; Kawaguchi, A.; Hasegawa, H.; Kajino, K.; Ninomiya, T.; Ijiro, K.; Sawa, H. Gold Nanoparticles as a Vaccine Platform: Influence of Size and Shape on Immunological Responses In Vitro and In Vivo. *ACS Nano* **2013**, *7*, 3926−3938.

https://dx.doi.org/10.1021/acsanm.0c01978
ACS Appl. Nano Mater. 2020, 3, 8557−8580